NUMERICAL MODELLING AND EXPERIMENTAL INVESTIGATION OF CFRP STRUCTURES FOR LARGE DEFORMATIONS

A Thesis

Submitted to the Faculty

of

Purdue University

by

Archit M. Deshpande

In Partial Fulfillment of the

Requirements for the Degree

of

Master of Science in Mechanical Engineering

August 2019

Purdue University

Indianapolis, Indiana

THE PURDUE UNIVERSITY GRADUATE SCHOOL
STATEMENT OF COMMITTEE APPROVAL

Dr. Hamid Dalir, Chair

Department of Mechanical and Energy Engineering

Dr. Andres Tovar

Department of Mechanical and Energy Engineering

Dr. Mangilal Agarwal

Department of Mechanical and Energy Engineering

Approved by:

Dr. Jie Chen

Head of the Graduate Program

I dedicate this to my parents.

ACKNOWLEDGMENTS

Firstly, I would like to express my sincere gratitude to my advisor Prof. Hamid Dalir for the continuous support of my Masters study and related research, for his patience, motivation, and immense knowledge. His guidance helped me in all the time of research and writing of this thesis. I could not have imagined having a better advisor and mentor for my Masters study.

Besides my advisor, I would like to thank the rest of my thesis committee: Prof. Andres Tovar and Prof. Mangilal Agarwal, for their insightful comments and encouragement, but also for the hard question which incented me to widen my research from various perspectives.

My sincere thanks also goes to Prof. Wallace, Mr. Alex Timmerman, and Mr. Craig McCarthy, who provided me an opportunity to access the laboratory, research facilities and manufacturing shop. Without they precious support it would not be possible to conduct this research.

I thank my fellow labmates in for the stimulating discussions, for the sleepless nights we were working together before deadlines, and for all the fun we have had in the last two years.

Last but not the least, I would like to thank my family: my parents and to my brothers and sister for supporting me spiritually throughout writing this thesis and my life in general.

TABLE OF CONTENTS

LIST OF TABLES

LIST OF FIGURES

Figure Page

ABSTRACT

Deshpande, Archit M. M.S.M.E., Purdue University, August 2019. Numerical Modelling and Experimental Investigation of CFRP Structures for Large Deformations. Major Professor: Dr.Hamid Dalir.

The use of carbon-fiber reinforced composite materials is not novel in the field of motorsports industry. Their use in collapsible structures for crashworthiness is however not fully understood and predicted. Due to the complex failure mechanisms occurring within the material, the energy absorbing capacity cannot be easily predicted. The need to understand their contributions in crashworthy structures is thus of great importance. Furthermore, failure of carbon-fiber composites is highly dependent on the geometry of structure. Problems arise in both experimental and numerical modelling of these structures. Although many explicit FEA codes exist, they often include experimental parameters that need to be calibrated through either coupon tests or actual crash tests. As composite structures become more commonly used in automotive industry, it is necessary to set some guidelines to successfully model and simulate composite crashworthy structures.

The numerical modelling was done in LS-DYNA Enhanced composite damage MAT54. The material properties were configured using experimental coupon tests. The tests were conducted on square composite tubes. The Specific Energy Absorption (SEA) of the tubes were calculated through several coupons. As SEA is a function of geometry, it was necessary to conduct tests with similar geometry as seen in nosecone. MAT54 was chosen to simulate both crush and crash simulations due to its capability to simulate element level crushing. Furthermore, various modifications within the material model, improve its accuracy to determine composite failure.

The research utilizes the characterization of material inputs in MAT54 by conducting quasi-static compression tests on simpler but similar geometry. By utilizing inputs, a zonal optimization was conducted on the nosecone geometry. The number of layers, layer orientations and ply thicknesses were varied to vary the energy absorbed per zone. The deceleration of the vehicle can thus be controlled, and the weight of the structure could be reduced.

1. INTRODUCTION

The superior performance qualities of Carbon fiber reinforced composites make them an ideal material to be used in the structures of automobiles and in motorsports. For CFRP to be utilized as a primary vehicle structure, the energy absorption capacity of the material should be predictable. As the failure of composite structures cannot be easily predicted due to their complex failure mechanisms, further research in design and simulation understanding need to be conducted. If composite vehicles structures are to be mass produced for occupant safety, they need to be better than their metallic counterparts. A superior chassis or structure with lower mass needs to still meet the crash certification requirements of either the motorsport governing body or automotive road safety standards.

The safety standards can be broadly summarized in the following manner. (1) absorbing or deflecting input kinetic energy, (2) controlling occupant deceleration, (3) utilizing collapsible structures, and (4) allowing for a safe post-crash egress. The deformation in a crash needs to satisfy the above set of regulations as they determine the survival of the occupants. Structural components designed for crashworthiness increase the energy absorption rate and hence increase the survivability of driver or occupants. Almost all modern automotive can be found with collapsible structural tubes or rails [1] [2] [3] [4] . The material attributed to these structures is mainly steel or Aluminum. These are ductile isotropic metals which fail in plastic regime by folding. The fold geometry or absorption rate can be easily and accurately determined due to the isotropic lattice structures of the material. In composites however, the failure is complex. Depending on the geometry, one or more than one of the following failures can occur, fiber fracture, matrix shear, fiber-matrix debonding, delamination [5]. Due to this reason crash structures often require experimental testing which would determine the accuracy and feasibility of the structure.

While experimental testing is conducted on every modern vehicle, the reliance of automotive industry on the capacity of FEA codes to accurately predict and observe energy absorption capacity for metallic structures cannot be neglected. By designing, optimizing and simulating different crash scenarios the expensive cost of crash testing prototypes can be avoided. Various other parameters like velocity, impactor angle, materials can also be varied to reduce the cost whilst increasing the safety of occupants. Thus, simulation has now been an integral part of certification process due to its ability to accurately depict the failure in metallic structures [6] [7].

The use of composites is expected to rise each year with a higher need for weight reduction. As more stringent rules are imposed on the vehicles each year to reduce the emissions, a lighter chassis would make a feasible choice. Furthermore, as there is a decrease in cost of carbon-fiber composite material, there is a higher demand within the automotive and aerospace industry. In order to design an optimum structure, and utilize the complete performance of composites, there needs to be a better understanding of energy absorbing mechanism and its inclusion within the numerical modelling or FEA codes. The research conducted here utilizes some novel experimental energy absorption characterization techniques and addresses some short comings of the methodology. The objective of this research is to (a) demonstrate and verify an experimental energy absorption characterization of composite system (b) utilize results in development of accurate model (c) determine the optimum ply stacking sequence for FIA regulations (d) compare the usage of this monolithic structure with other sandwich structures (e) address the shortcomings of this methodology.

2. LITERATURE SURVEY

The research to understand the failure mechanisms and the absorbed energy began in 1980s. To this day researchers havent been able to attribute the failure modes for a geometry because of the complex and technical challenges involved. Hence, the development of components is dependent on experimental results and their investigation. In order to understand the variations in Specific Energy of Absorption (SEA), there is a need to understand the generalized crushing behavior and the variations in Reaction Forces with crushing displacements. Most structural CFRP components are manufactured using a thermoset matrix, namely epoxy. Thus, this research review would focus only on thermoset resin. The resultant composite structures are brittle and ideally fail by fragmentations/chipping. As shown in Figure 2.1, a square cross-sectional tube undergoes progressive crushing. The typical resultant force-displacement curve

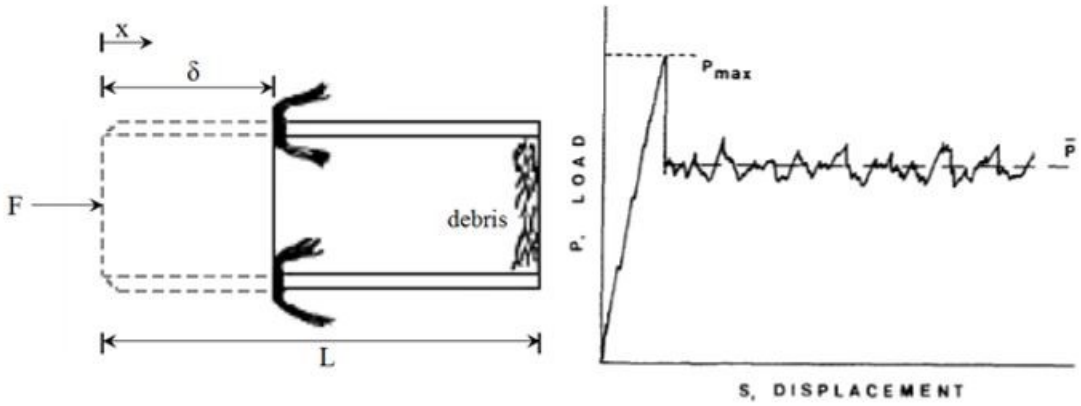

Fig. 2.1. Schematic of composite tube with a chamfered crush initiator undergoing progressive crushing and the resulting load-displacement crush curve, from Hull [5].

is observed in Figure 2.1. The schematic features a chamfered start which is known as crush trigger. The crush trigger initiates progressive stable crushing. In an absence of crush trigger, the structure buckles and very high initial force peaks are observed. The energy absorbed in structure is the area under the force-displacement graph. If the structure buckles, the initial peak force is very high, but the net energy absorbed is low. Hence, a stable and progressive crushing is desired to absorb maximum amount of energy.

The force stabilizes once progressive crushing is initiated. The average force is calculated by averaging the force in progressive crushing zone. The Energy absorbed can thus be given by,

$$EA = \int_0^{\delta} F.dz \tag{2.1}$$

The Specific Energy Absorbed is defined as the energy absorbed per unit mass of material and has units as J/gms. Thus, SEA can be given as,

$$SEA = \frac{EA}{m} = \frac{\int_0^{\delta} F.dz}{\rho.Vol} \tag{2.2}$$

The SEA of material is usually defined to depict the performance capabilities of a particular material. It quantifies the maximum crush performance which can be utilized while designing of components.

Most research conductor previously focuses on axial compression of thin walled composite tubes. Hull [5], provided some perspective on the complexity of failures involved in CFRP crushing. He identified two main modes of failures, fragmentation and splaying. Many interrelated parameters of the geometry define the nature of progressive crushing. The relation between these parameters is dependent on the structure, trigger, material and temperatures and hence concluding the research as inconclusive.

Farley and Jones [8] developed the first understanding of failure mechanism in stable crushing. They concluded three fundamental crushing modes. These modes are transverse shearing, brittle fracturing and lamina bending. In later publications

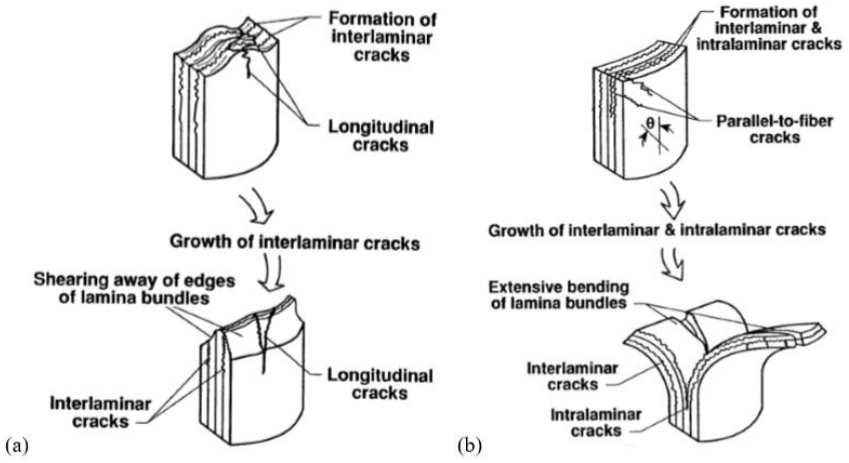

Fig. 2.2. Farley and Jones failure modes (a) transverse shearing (b) lamina bending

the brittle fracturing mode was concluded as a combination of lamina bending and transverse shearing [9]. These results are similar to the conclusions of research conducted by Hull [5]. As shown in Figure 2.2 (a), there is formation of cracks both lateral and longitudinal to fiber directions. These cracks divide the crush front into various lamina bundles each subjected to transverse shearing. The number of cracks and amplitude of cracks are a function of structure and material. The principal energy absorption mechanism was attributed to this transverse shearing. Figure 2.2 (b) depicts the lamina bending failure mechanism. There is formation of cracks parallel to layer of fibers. As the cracks are non-intersecting, the lamina bundles formed are not subjected to transverse shearing and instead subjected to bending. This does not result in fiber breakage which absorb large amount of energy. Thus, this failure mechanism was described as an inefficient crushing mode by the researchers.

Following the work conducted by Farley and Jones, Hull [5] suggested eight different failure mechanisms for composite crush. Hull identified tension, compression and shear for fibers, in both lateral and longitudinal directions, and interlaminar failures in shear and tension. The failures were generalized into two modes as fragmentation

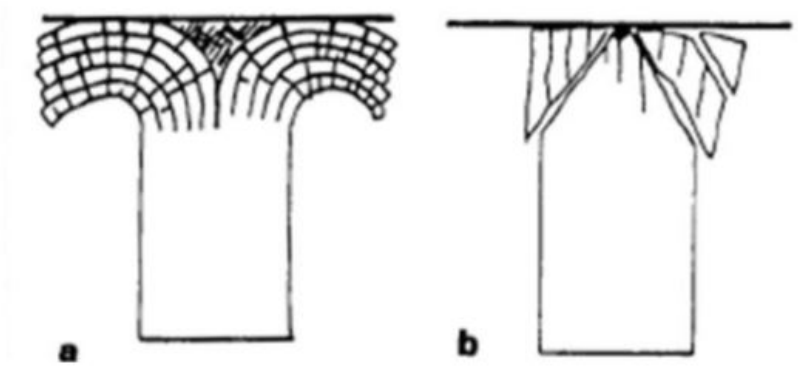

Fig. 2.3. Failure modes suggested by Hull [5], (a) splaying and (b) fragmentation

and splaying. A progressive failure is a combination of both with dominance of one particular mode dependent on other parameters. Splaying is a result of formation of long cracks between plies in the matrix, which leaves most fibers intact. Fragmentation failure is characterized by fiber fractures and matrix shear which renders the material as debris. The research suggests the arrangement of fibers plays an important role in determining the dominant failure mode for crushing. An increase in ratio of hoop fibers in specimen increases the dominance of fragmentation as the axial splayed fibers are withheld within the hoop fibers till fragmentation occurs. The research conclusion is applicable to structures which have a closed cross-section as open cross-sections would not contain the lateral deformations. The two modes are shown in Figure 2.3.

Carruther [10] also conducted several experimental tests on composite crush tubes. He concluded, of the many failure mechanisms, the most dominant include transverse shearing, brittle fracture, lamina bending, lamina separation, and buckling. He further concluded that the previous research conducted identified the extreme failure modes (by both Hull and Farley), splaying and fragmentation. Furthermore, he concluded that the energy absorbed in fragmentation mode is higher than in splaying mode and refers to work conducted by Hamada [11]. The research also suggested

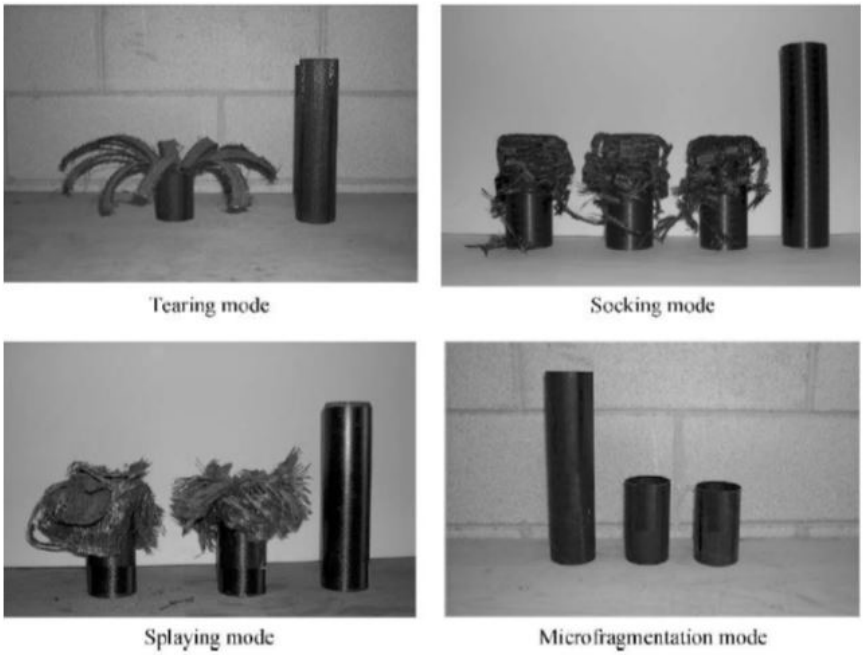

Fig. 2.4. Failure modes suggested by Bisagni [3]

that the dominant failure mode was dependent on factors such as the material, lamina angle, specimen geometry, stacking sequence and the testing speed.

Bisagni [3] also conducted some compression tests on circular thin walled tubes. He observed four failure modes namely, microfragmentation, splaying, socking and tearing. The socking and tearing failure modes were attributed as a combination of fragmentation and splaying as suggested in previous research. The observed failure modes are shown in Figure 2.4.

Most fundamental research for understanding the failure mechanisms in composite was limited to the above research. While there is a general consensus amongst all researchers, the parameters affecting the dominance of the failure mode is conflicting. However, the common conclusion for all research is there are different failure modes occurring simultaneously, but they are a combination of the two fundamental failure modes, transverse shearing/fragmentation and lamina bending/splaying. The

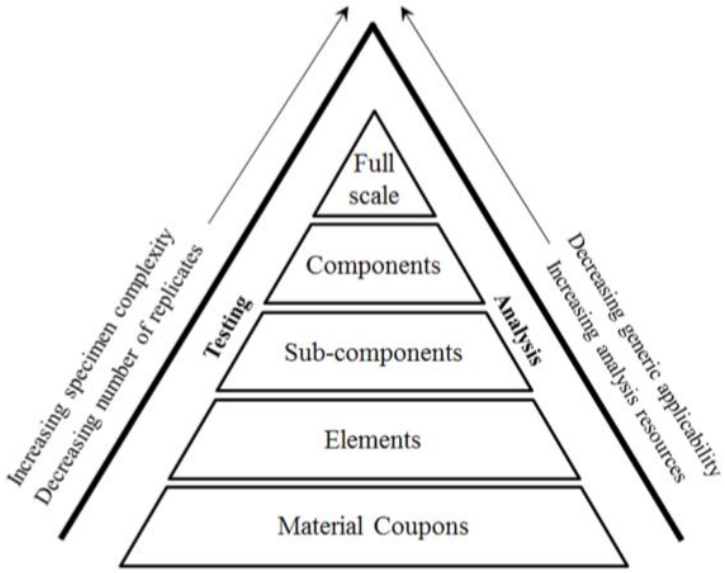

Fig. 2.5. Building Block Approach

dominance of the first failure mode increases the energy absorbing capacity of the structure and hence should be dominant.

Over the past decade, the automotive industry has relied exclusively on the use of modern FEA codes specifically designed for large deformations. These include LS-DYNA, Abaqus, RADIOSS and PAM-Crash. Given the technical challenges involved in composite crushing, full-scale FEA crash requires a different methodology to predict energy absorption as compared to its metallic counterparts. Building Block Approach (BBA) is one such method which enables composite damage material models to be utilized for simulating crash scenarios. It is defined in greater detail in CMH-17 handbook [12]. The BBA was developed to assist the design and simulation of composite structures and optimizing the structures with minimum resources.

As suggested in Figure 5, the BBA utilizes simpler material coupons at the start of process. As the complexity of parts increases from coupons, structural elements to full scale models; the need of testing and analysis decreases. Each increment in level, increases the size and complexity of structure to be designed and is based on

the knowledge acquired in previous step. Hence the full-scale model does not require multiple analysis runs or crash tests to verify and predict the energy absorbed.

The numerical modelling of crash is always conducted at an element level. The FEA code utilizes explicit formulation, which is discussed in further details, later in this report. The explicit calculations are stable but computationally expensive [13] [14] [15] [16]. The utilization of solid elements is thus not ideal. The shell elements utilize 4 orthotropic nodes as compared to minimum of 8 in solid elements. Maia and Oliveria [16] concluded the reliability and usefulness of 4 node Belytschko-Tsay elements in their research. The elements reliability on local coordinate system for reducing errors in stresses and strains made them the ideal element type to be utilized for composite large deformation simulations. Each ply is represented by an independent integration point within the element. This reduces the computational requirements for any contacts between the plies while simulating the interlaminar behavior. For models where lamina separation is necessary, tiebreak contacts can be developed which simulate the delamination.

The crash modelling strategy utilized in this research would include the use of MAT 54 (Enhanced composite damage). The material model is traditionally considered as the benchmark for composite crash in both aerospace and motorsport industry [17] [18] [19]. It utilizes the failure of fiber and matrix in shear by Chang-Chang failure criterion. The details are covered further in this report. The material model is chosen for its minimal inputs which can be obtained in basic testing facilities with relative ease and accuracy. Furthermore, the model is specifically designed for shell elements in full-scale crash model which further aids in the BBA methodology. Also, Feraboli [20], utilized this model successfully, and with accuracy, for similar simulations. By utilizing MAT 54 with Belytschko-Tsay elements, the energy absorbed is varied.

3. EXPERIMENTAL

3.1 Coupon Material

As mentioned earlier, the motive of experimental testing is to measure and characterize the energy absorption capability of composite system. The results would be used further in the BBA approach in designing the composite parts. The material utilized for this study is CFRP SC110(T2) 2X2 twill prepreg from Gurit Holding. The prepreg is infused with resin which is cured at a temperature of 120C for 60 minutes. Quasi-static compression tests are conducted for square coupons with an intention of calculating the Force variations with displacement of material while keeping various other parameters like layup, trigger, manufacturing process and other testing parameters constant. The layup for each square tube was considered to be $[0/90]_{2_S}$ which yields a final cured thickness of 1 mm. The material properties are provided in the table below.

Table 3.1.: Material Properties of CFRP SC110(T2) 2X2 twill prepreg

Property	Value
X_t	794 MPa
E_{t_1}	69 GPa
X_c	796 MPa
E_{c_1}	66 GPa
Y_t	766 MPa
E_{t_2}	72 GPa
Y_c	775 MPa

continued on next page

Table 3.1.: *continued*

Property	Value
E_{c_2}	65 GPa
S_c	73 MPa
G_{1_2}	4.2 GPa

3.2 Coupon Geometry

The coupon compression tests were carried on square cross-sectional specimens. The length of specimen was 171 mm and each side measured 27.4 mm. The corners were filleted with 3.2 mm radius hence reducing the stress concentration on the edges. A 45 chamfer was included at the top edge to initiate crushing behavior, as is a common practice in composite coupon tests. All tests were performed at a rate of 4 mm/sec which is below the critical speed of 1 m/s. The specimen before crushing is shown in Figure 3.1.

Fig. 3.1. Square tube specimen for coupon tests

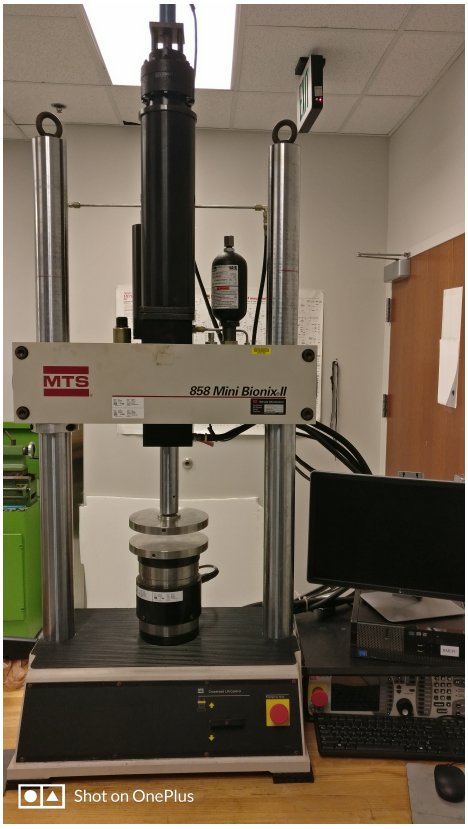

Fig. 3.2. Compression Test Rig 858 Mini Bionix II

3.3 Compression Test Rig

The compression tests were conducted on testing rig from Material Testing System (MTS 858 Mini Bionix). The Force range for the testing system can be varied from 1 N to 25 KN. The specimen size for the above system is standard (200mm x 100mm) with maximum displacement of 80 mm. The tests were conducted on flat bed with a displacement rate of 4 mm/sec. The system is hydraulically actuated with an accuracy of 0.1 N. The compression testing rig is shown in Figure 3.2. The displacement and force applied were recorded with a frequency of 20 Hz.

Fig. 3.3. Crushed square specimen

3.4 Compression Test results

The experimental results of the compression tests are shown in Figure 3.4 - 3.6. The crushed square specimen is shown in Figure 3.3. The tests were performed on 3 specimens of same dimensions. The results of each were averaged to calculate the forces exerted on the tube. The results were within 5-8% of average. These low variations indicate stable, repeatable and progressive crushing in the specimen. The energy absorption rate observed was similar to that suggested by Wade [21].

The SEA observed varies between 35 J/gm which is a good correlation with the previous observations of 37 J/gm [21]. While the material in the two studies differ, the effects of variation of curvature percentage in geometry is not of key interest. The results from other compression tests achieved similar test results hence by following the variations of SEA as a function of Φ from [21] we can estimate the SEA variations for the CFRP material. As the product been developed has a square cross-section, with similar curvature percentages, the effects of the variation in geometries is not included in this study.

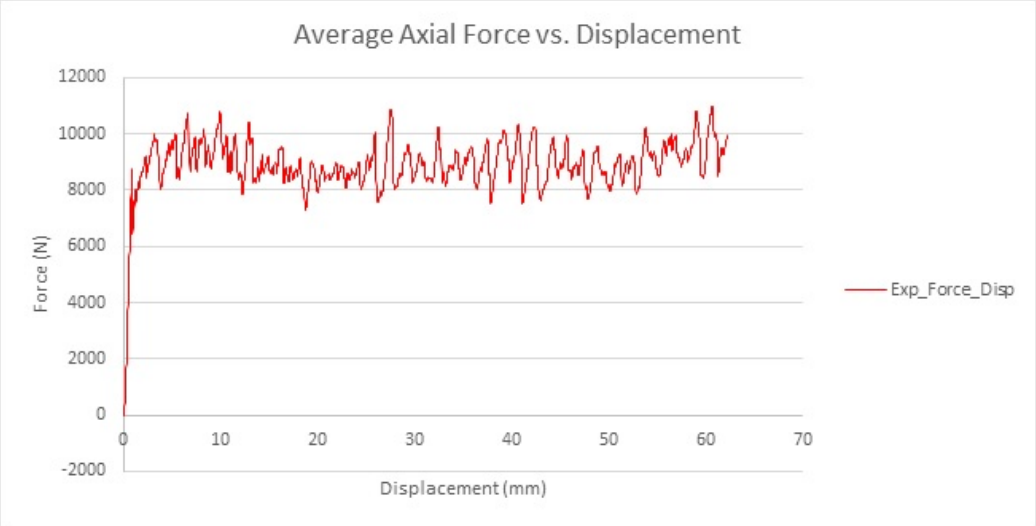

Fig. 3.4. Force Displacement data from compression of square specimen

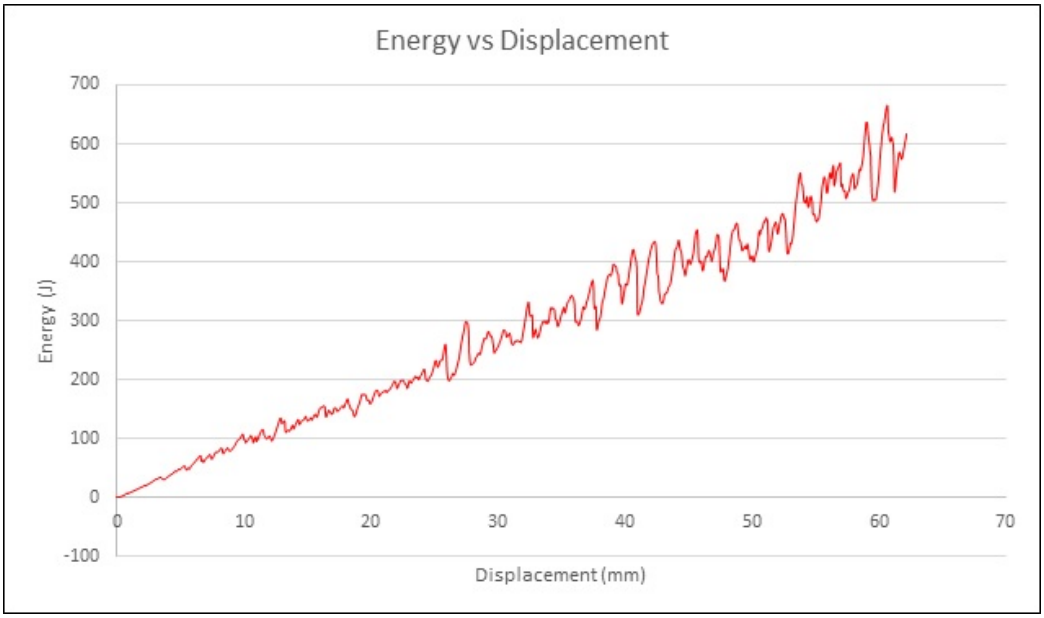

Fig. 3.5. Energy displacement data from compression of square specimen

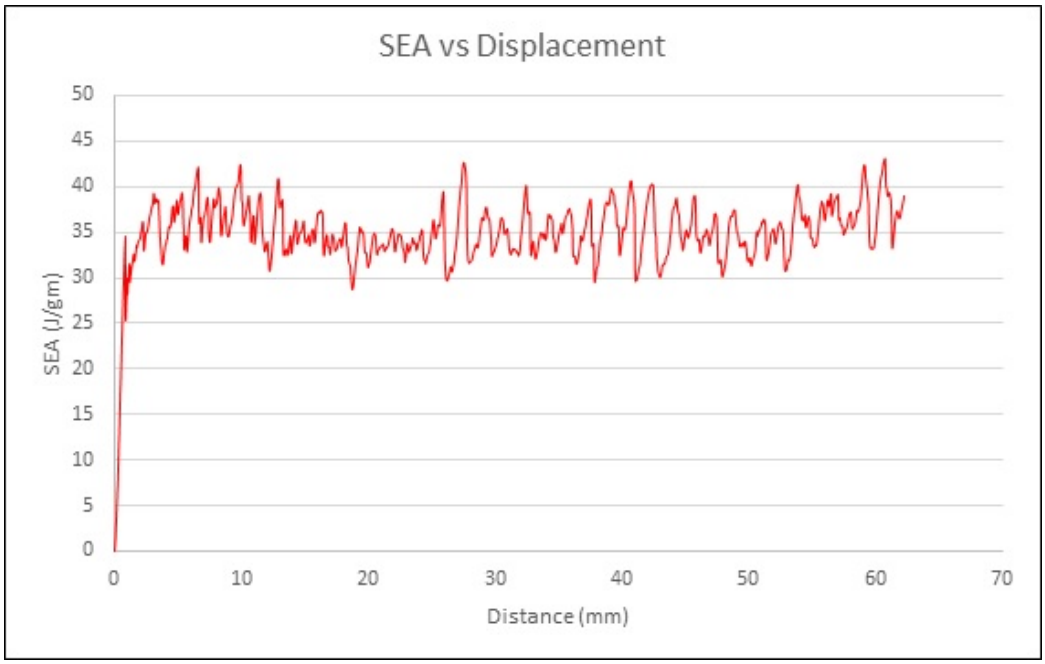

Fig. 3.6. SEA distance data from compression of square specimen

4. ANALYSIS

The aerospace and automotive industries have relied extensively on LS-DYNA MAT54 for explicit dynamic simulations. The material model is considered to be a benchmark for composite damage analysis due to its specific development for shell elements. Almost all explicit simulations in composites utilize shell elements for their reduced computational cost and fewer input parameters. The details are further explained in LS-DYNA Users Manual [22]. As the material model is of great interest, it is necessary to understand the input parameters necessary for the model. MAT 54 input parameter definitions are mentioned in Table 4.1.

Table 4.1.: MAT 54 Input Parameters

Definition	Type
MID: Material Identification Number	Computational
ρ: Density of material	Experimental
E_a: Youngs Modulus (0°)	Experimental
E_b: Youngs Modulus (90°)	Experimental
ν_{b_a}: Poissons ratio in AB direction	Experimental
G_{a_b}: Shear Modulus	Experimental
DFAILM: Transverse Matrix failure strain	Experimental
DFAILS: Shear failure strain	Experimental
DFAILT: Tensile fiber failure strain	Experimental
DFAILC: Compressive fiber failure strain	Experimental
TFAIL: Timestep for element deletion	Computational
Alpha: Shear stress parameter	Damage dependent
Soft: Strength reduction factor	Damage dependent

continued on next page

Table 4.1.: *continued*

Definition	Type
FBRT: Reduction factor for X_t	Damage dependent
YCFAC: Reduction factor for X_c	Damage dependent
EFS: Effective failure strain	Computational
X_c: Compressive strength (0°)	Experimental
X_t: Tensile strength (0°)	Experimental
Y_c: Compressive strength (90°)	Experimental
Y_t: Tensile strength (90°)	Experimental
S_c: Shear strength	Experimental
β: Shear factor for fiber tensile failure	Damage dependent
PEL: Percentage of layer failure	Damage dependent

A parametric study was conducted for the above parameters. Although the basic material properties were presented in the material datasheet, there is a need to understand the effects of variation of the input data to better correlate the simulated results with the actual experimental results. Furthermore, various parameters require experimental results to reduce the error percentage and better predict the results. The properties in Table 4.1, which are damage dependent, are properties that vary as per the material and hence require sensitivity analysis. Other parameters like TFAIL are required in simulation only, as these would be utilized to delete the elements. Without the timely deletion of elements, there is a loss in input energy which is not present in experimental results.

The shell elements are attributed with the composite material model by utilizing Part_Composite input deck. Each ply properties are attributed to the particular shell element by creating an integration point through the thickness (Figure 4.1). The integration points can be created above, below or midway to the shell element position in the global coordinate system. Each ply properties like ply thickness, ply

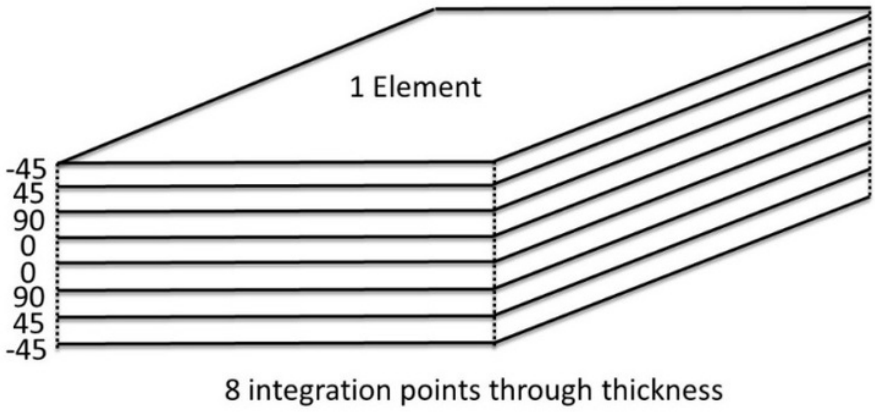

Fig. 4.1. Through-Integration points defined in a shell element

orientation to local coordinate system, ply material and ply thermal properties can be varied and attributed to the integration point.

The LS-DYNA simulation model is represented in Figure 4.2. A loading plate of certain mass is imparted constant velocity by utilizing Prescribed_Motion_Rigid. There is no reduction in velocity of loading plate with the development of resistive contact forces. The figure also shows two separate sections in the square tube. The first row of elements act as a trigger to the other specimen. The introduction of trigger enables progressive crushing. The geometry is imported from a CAD software and meshed in LS-Prepost. The geometry was meshed into fully integrated shell elements of 2mm x 2mm size. The laminate thickness developed was 1.016 mm by utilizing 4 plies each of 0.254 mm thickness. As 4 plies are defined, there are 4 integration points. The total number of elements modelled were 5164 each of 1.016 mm thickness.

The input values for parameters in material model MAT 54 are shown in Figure 4.3. The units need to be consistent with LS-DYNA Consistent Units. For the case of presented simulation, the consistent units are presented in Table 4.2.

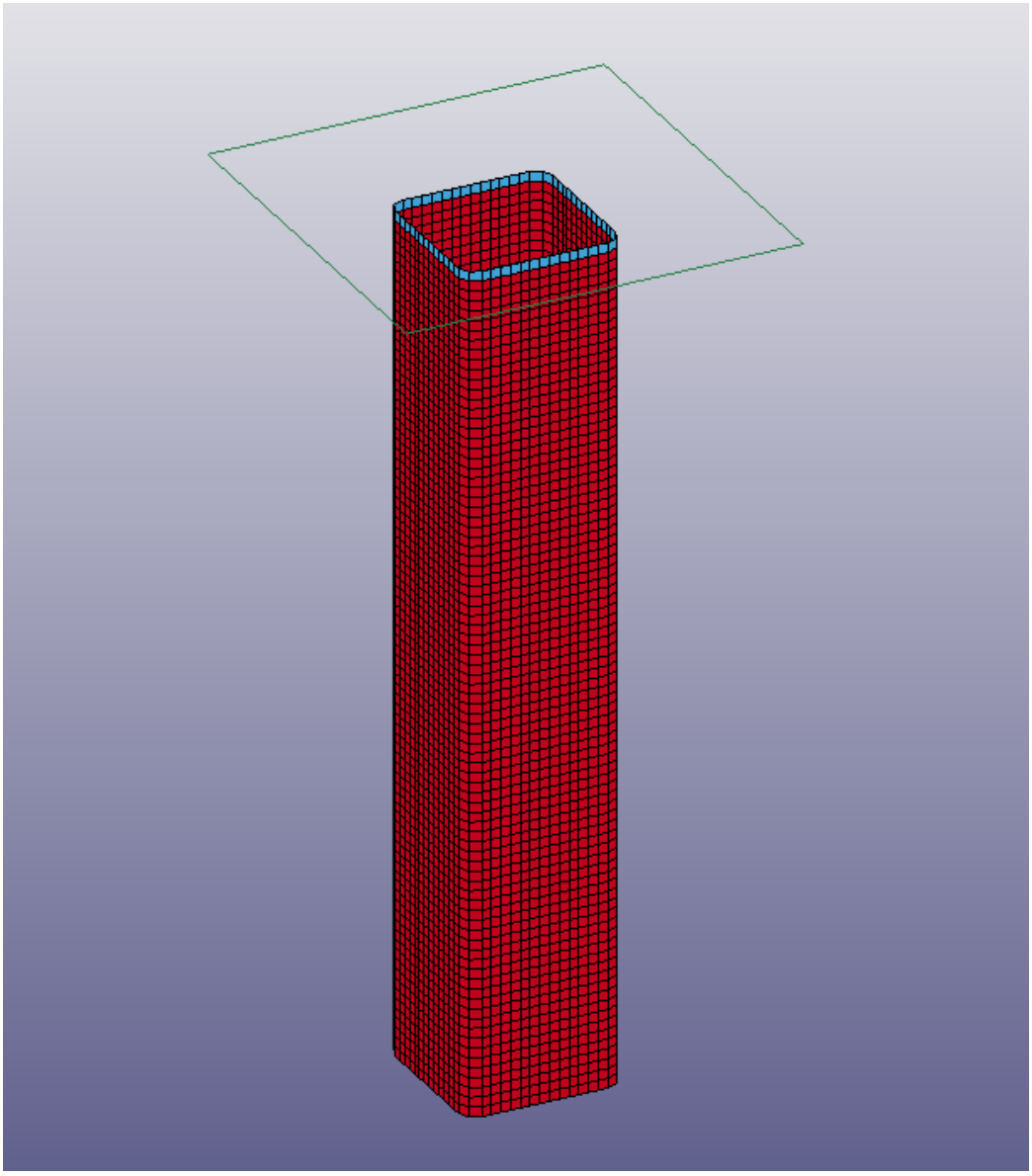

Fig. 4.2. LS-DYNA model of square tube subjected to quasi-static compression

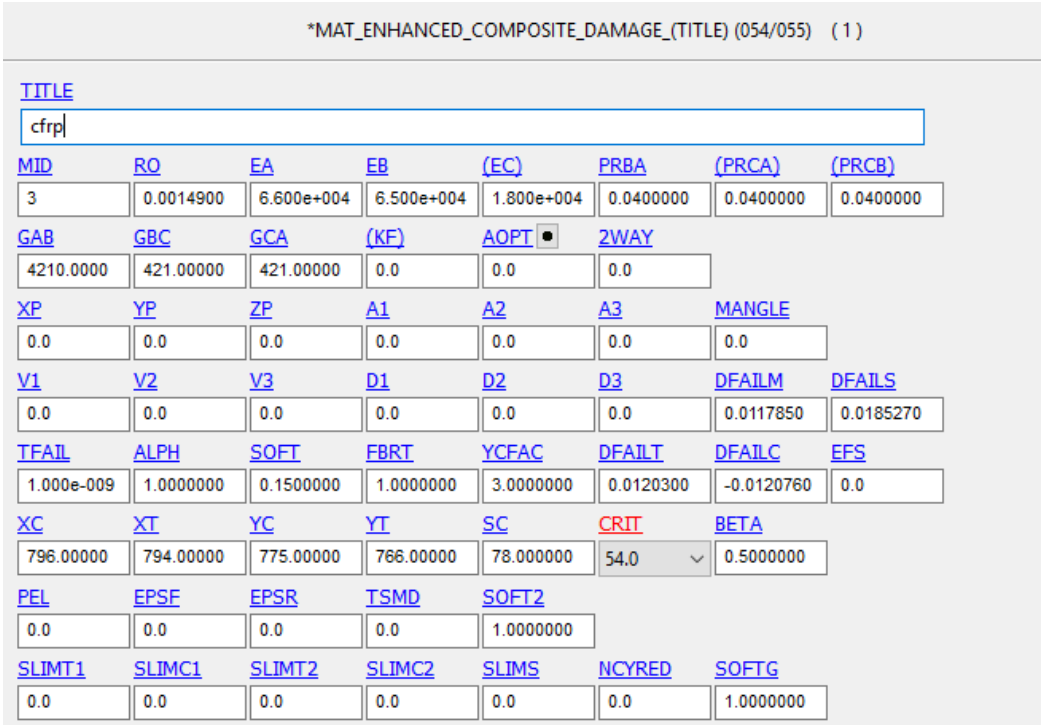

Fig. 4.3. LS-DYNA MAT 54 Input Parameters for quasi-static compression tests

Table 4.2.: LS-DYNA Consistent Unit

Definition	Type
Mass	Grams (gms)
Length	Millimeter (mm)
Time	Millseconds (ms)
Force	Newtons (N)
Stress	MegaPascals (MPa)
Energy	Newton-Millimeter (N-mm)

The trigger for the square tube is modelled as a single step with a thickness of 0.2 mm. In order to model the trigger, it is defined as a separate part with independent ply thickness and layup. A contact definition is established within the trigger and the rest of the specimen. Contact_Automatic_Single_Surface is defined with both parts

as slaves hence merging the two parts into a single entity, each failing independently. The square tube is kept stationary with no Degrees of Freedom at the bottom set of nodes.

The contact between the loading plate and specimen is necessary to accurately predict the interaction with the Rigid body. While many previous researches utilized Contact_Automatic_Suface_to_Surface, there is sudden loading onto the specimen. In order to prevent the impact loading, Rigid_nodes_to_Rigid_Body is utilized. While this type of contact is generally utilized with non-deformable structures, a loading curve can be defined which would accurately predict the force transfer at the interaction. The loading curve defines the force generated by contact springs as a function of penetration. The stiffness of the penalty springs and frictional springs are generated by trial and error and hence cannot be formulated for complex structures. The material model utilized for loading plate is MAT 20 Rigid. This is a typically utilized for loading plates as it does not consider the deformations or stresses induced within the body and hence reduces computational requirements. The timestep for explicit calculations is not considered as LS-Dyna calculates the minimum timestep as per Courants criterion [23]. Also, the total simulation time varied between 150-175 seconds for each run on a 64-bit 8 core 4.2 GHz processor.

The results of baseline simulation reveal that the collapse of square tube is even and stable. There is stable and progressive crushing which is necessary as the experimental compression results also indicate the same failure mechanism. Although in simulations, the failure of elements differs to what is actually observed in experiments. When a ply fails in element, the element does not deform due to a change in ply damage which is not observed in experiments. The element fails once there is failure of all layers of element. Once a particular element fails in a row of elements, the entire row of elements is deleted as per TFAIL which is observed only in simulations. Furthermore, in MAT 54 there is no delamination considerations which further differentiates the results from experiments. However, the effect of SOFT compensates for all such inaccuracies. Hence it is important to correlate the coupon test results

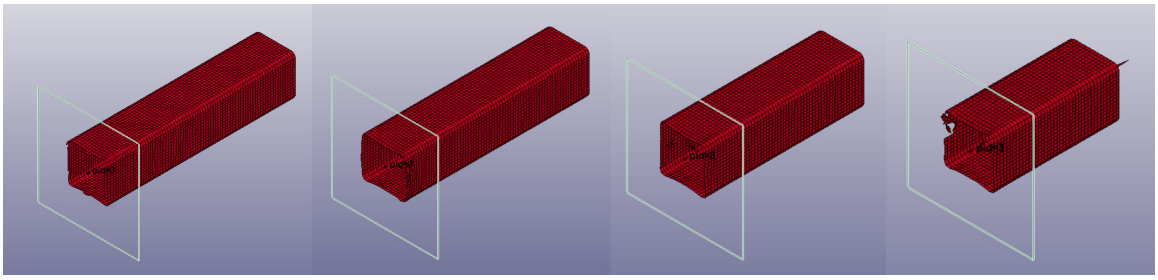

Fig. 4.4. Progressive compression of composite square tube in LS-DYNA

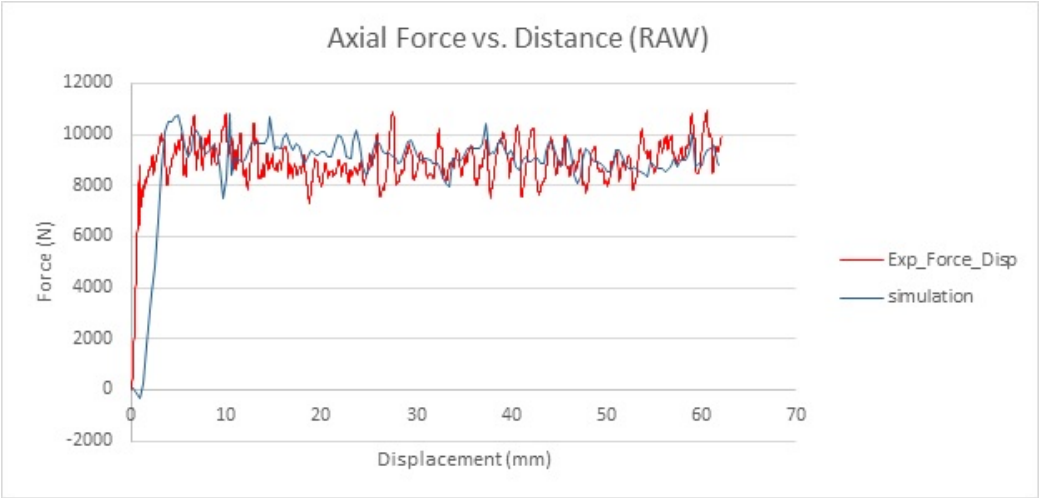

Fig. 4.5. Experimental and Simulation load curves for quasi-static compression

with experiment to accurately predict the failure of more complex structures. The failure of specimen is shown in Figure 4.4.

As can be observed in Figure 4.5, there is a good correlation between the simulation results and experimental results. The simulation model closely resembles and predicts the experimental data and is able to capture the effects and features observed. The error percentage varies within 5% which is the acceptable range for simulation errors and hence the final material model can be successfully utilized for the final geometry.

The simulation results were not directly correlated. Extensive parametric studies were conducted to understand the behavior of composite material and the effect of each parameter on the force-displacement curve. Table 4.3 mentions the parametric studies (Sensitivity Analysis) conducted to obtain the end simulation results.

Table 4.3.: Parametric studies conducted in MAT 54

Parameter	Parametric Variations
MAT 54: XT	714.6, 595.5, 397, 158.8, 79.4, 873.4, 992.5, 1191, 1429.2
MAT 54: XC	716.4, 676.6, 597, 398, 79.6, 875.6, 915.4, 995, 1194, 1512.4, 1592
MAT 54: YC	697.5, 658.75, 387.5, 77.5, 852.5, 891.25, 1162.5, 1472.5, 1550
MAT 54: YT	689.4, 651.1, 383, 76.6, 0, 842.6, 880.9, 957.5, 1455.4, 1532
MAT 54: SC	0,7.8,39,97.5,58.5,89.5,156, 148.2, 117, 89.5, 66.5, 85.8, 70.2
DFAILT	0, 0.005, 0.00625, 0.0075, 0.01, 0.015, 0.017, 0.02, 0.03, 0.04, 0.06
DFAILC	-0.005, -0.0075, -0.00875, -0.01, -0.012, -0.015, -0.02
DFAILM	0 0.005, 0.01, 0.0125, 0.015, 0.02, 0.03, 0.04
DFAILS	0, 0.005, 0.01, 0.0125, 0.015, 0.02, 0.025, 0.03, 0.04, 0.05
EFS	0, 0.01, 0.025, 0.75, 1
ALPHA	0, 0.001, 0.01, 0.03, 0.3, 0.5, 0.9
BETA	0, 0.5, 1

continued on next page

Table 4.3.: *continued*

Parameter	Parametric Variations
TFAIL	1E-8, 1E-7, 1E-6, 1E-5, 1E-4
SOFT	0, 0.1, 0.15, 0.175, 0.25, 0.3, 0.5, 0.6
FBRT	0, 0.1, 0.2, 0.5, 0.6, 0.8, 1
YCFAC	0, 0.2, 0.5, 0.8, 1, 1.4, 1.6, 1.8, 2, 3, 4
CONTACT LOAD-CURVE	SOFT 1, SOFT 2, STIFF 1, STIFF 2
TRIGGER THICKNESS	0.05, 0.1, 0.15, 0.18, 0.3, 0.4
TRIGGER LAYUP	(0,0), (0,45), (45,45), (45,90)

4.1 Sensitivity Analysis

The simulation model should be able to accurately predict the failure of composite structure while accounting for minor changes within the input material properties. As the material properties presented in material data sheet are not calculated for the particular supplied material roll, there could be an error in the properties. Furthermore, the errors while manufacturing and data measurement of the material should not affect the design of end product. Hence it is necessary for simulation model to incorporate these errors and come up with a safe design. The following research presents the effects of varying the parameters as previously mentioned in Table 4.3.

4.1.1 Sensitivity Analysis of Strength

Effect of variation in MAT 54: XT

As is evident in Figure 4.6, the effects of varying XT from -90% to +90% has little effect on the crushing force requirements. The graph stabilizes to a certain value followed by failure by buckling. At extremely low values of XT (-90%), buckling failure is delayed which still has no significant effects on stabilized crushing force. Hence,

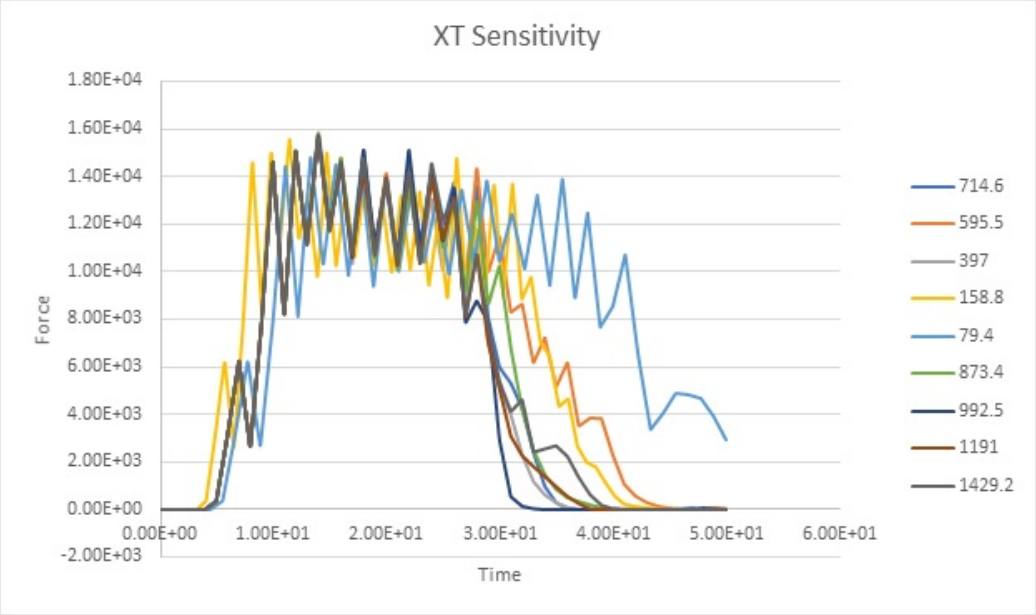

Fig. 4.6. Sensitivity Analysis of varying MAT 54: XT

we can conclude that the fiber tension failure has little effects on the primary failure mechanism involved in composite material and structure involved. Furthermore, the large reduction in strength value, changes the failure mechanism of composites from brittle failure to ductile failure which is incorrect.

Effect of variation in MAT 54: XC

The effects of varying compressive strength are shown in Figure 4.7. The sensitivity analysis conducted includes 10%, 15%, 25%, 50%, 90%, 100% increase and decrease in baseline value of 796 MPa. The effects of varying the compressive strength has drastic effects on resistive force generated. The failure mechanism also varies as a lower strength value changes the failure of composite from brittle failure to plastic failure. A large increase in compressive strength causes buckling of square tube followed by failure unstable failure. A small increment or decrement in XC has dramatic effects on failure of specimen. Hence, we can conclude the failure mechanism is dominated by compressive strength.

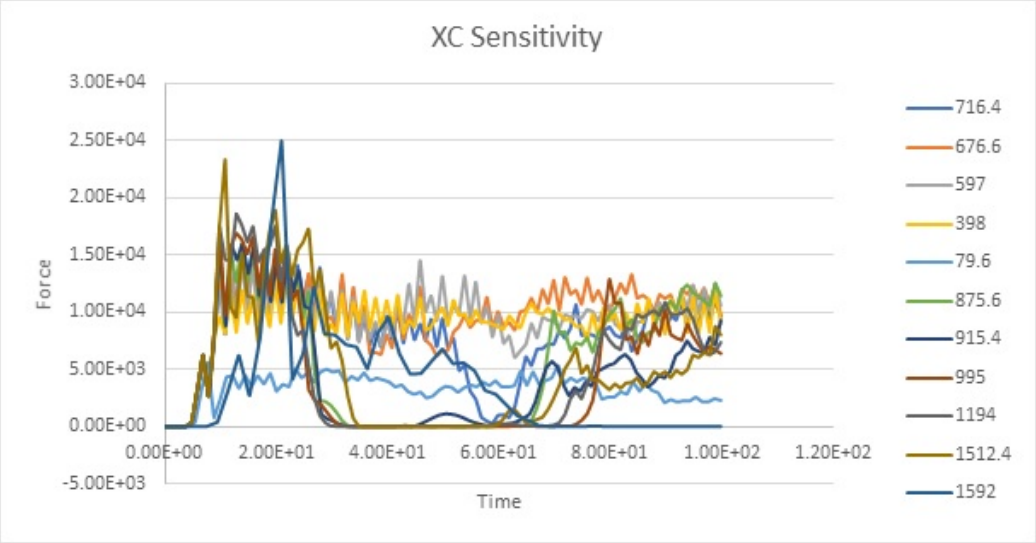

Fig. 4.7. Sensitivity Analysis of varying MAT 54: XC

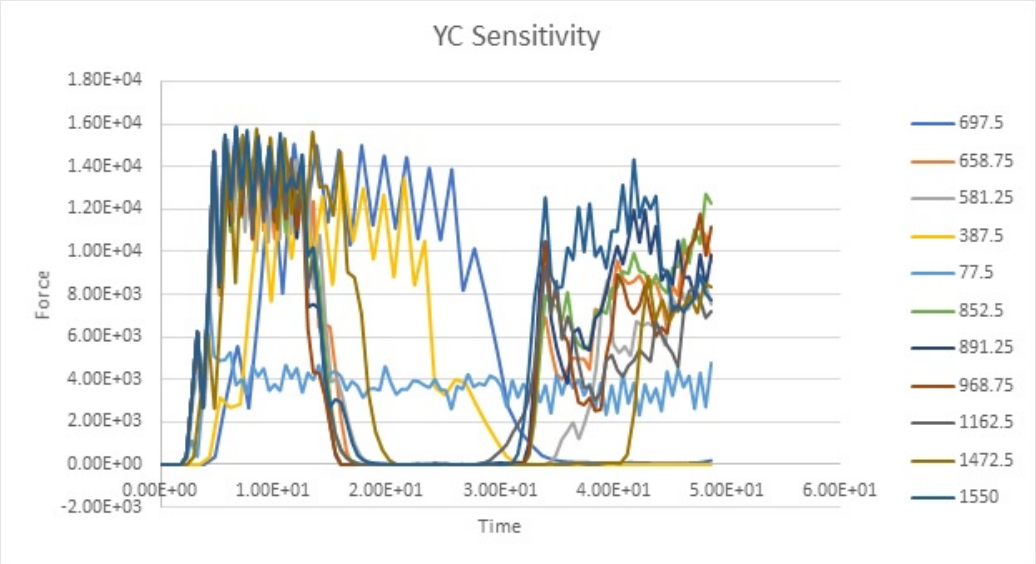

Fig. 4.8. Sensitivity Analysis of varying MAT 54: YC

Effect of variation in MAT 54: YC

The effects of varying compressive strength in E_{2_2} direction is shown in Figure 4.8. Although a fabric has almost similar strength in both directions, the positive increase in strength has little effects on the failure or resistive force generated. A decrement of 10% and 50% has slight overall improvement but the structure fails by buckling which is not observed in experiments. A reduction in strength by 90% has dramatic effects. There is stable failure but the failure changes from brittle to plastic which is incorrect. Hence, there is a need to vary other parameters to further capture the effects accurately as observed in experiments.

Effect of variation in MAT 54: YT

As can be observed in Figure 4.9, the variation of Tension failure strength in E_{2_2} direction has little effects on force-displacement curve and hence is not the primary factor for failure. Extreme changes in values has no significant effects so we can fix the failure strength to the baseline value.

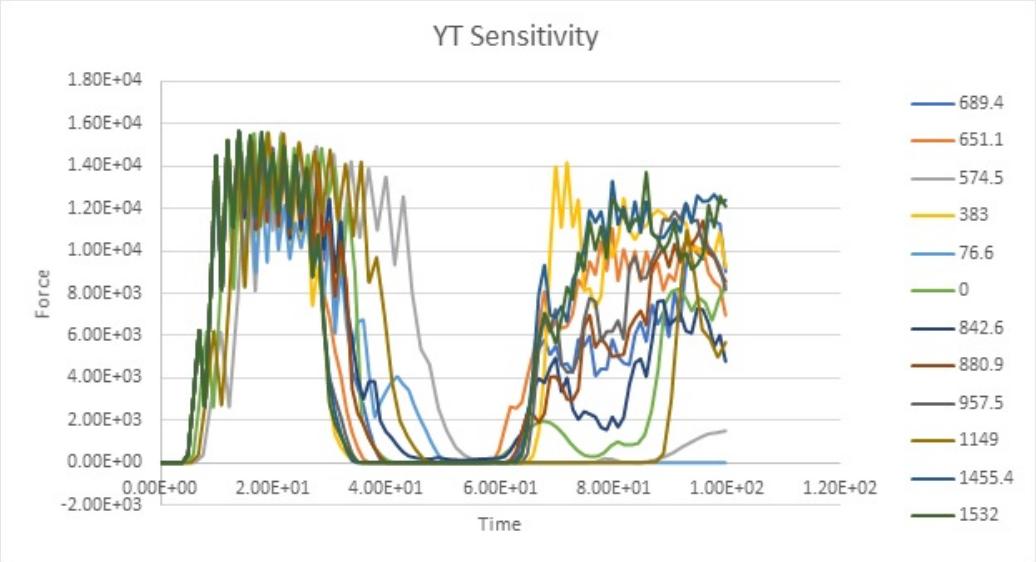

Fig. 4.9. Sensitivity Analysis of varying MAT 54: YT

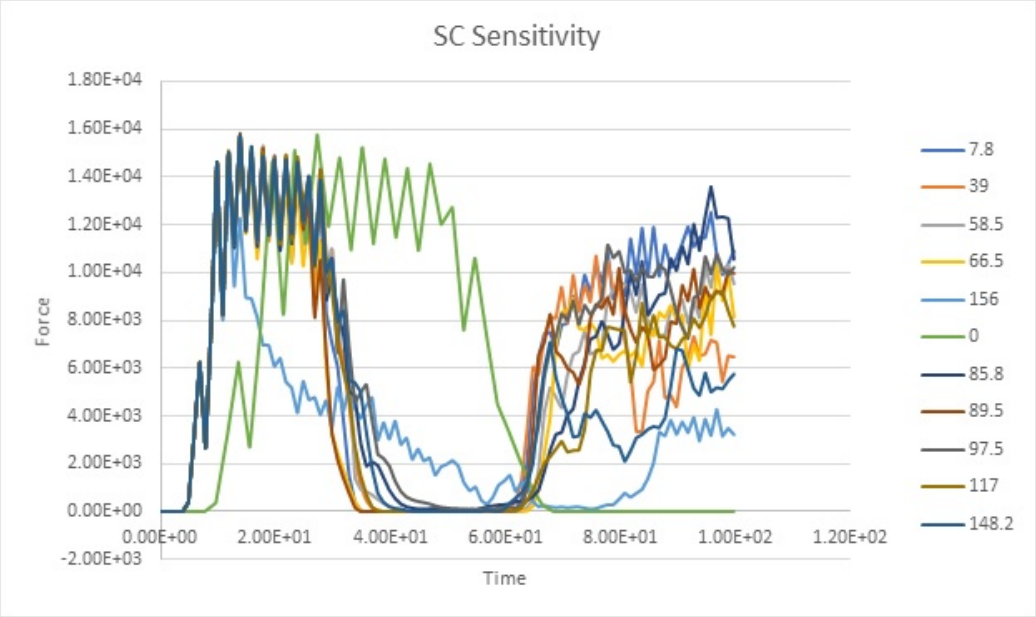

Fig. 4.10. Sensitivity Analysis of varying MAT 54: SC

Effect of variation in MAT 54: SC

Figure 4.10 shows the effects of variation in shear strength SC. Except for extreme variations in SC (-100% and +100%) the changes in shear strength has little effects on force-displacement curve. Furthermore, as the layup sequence does not incorporate 45 plies, the effects of shear strength variations were expected to be negligible. Hence, we can conclude that the shear failure is not a primary mode of failure and has no significant effects on simulations.

The effects of variations in strength have significant effects in compressive failure but little effects in tension or shear failure modes. Also, the change in strength values should be the last parameters to be varied as other parameters need to be configured correctly. The errors in strength generally vary within 5% of data provided and hence major changes should not be considered.

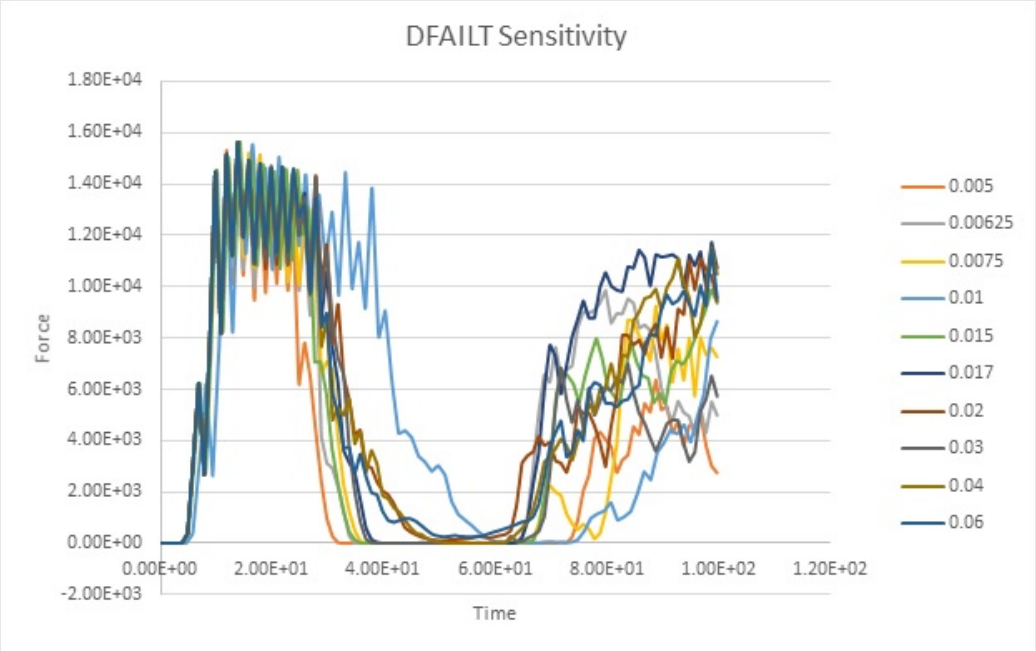

Fig. 4.11. Sensitivity Analysis of varying DFAILT

4.1.2 Sensitivity Analysis of Strain

Effect of varying DFAILT

Since the baseline values suggest failure by buckling, the effects of strain need to be observed. As the effects of tensile strength have negligible effects on simulation results, the effects of tensile strains too should have no significant effects. As is evident in Figure 4.11, the effects of DFAILT have low to none effects on force-displacement curves. As is evident in the figure, large variations have no effects.

Effect of varying DFAILC

The effects of compressive strains are significant on the simulation results. As compressive failure mode is the dominant factor, the variations in strain values have dramatic effects on structure and resistive force generated. As is evident in Figure 4.12, by increasing the strain value by 100%, the peak force on contact increases

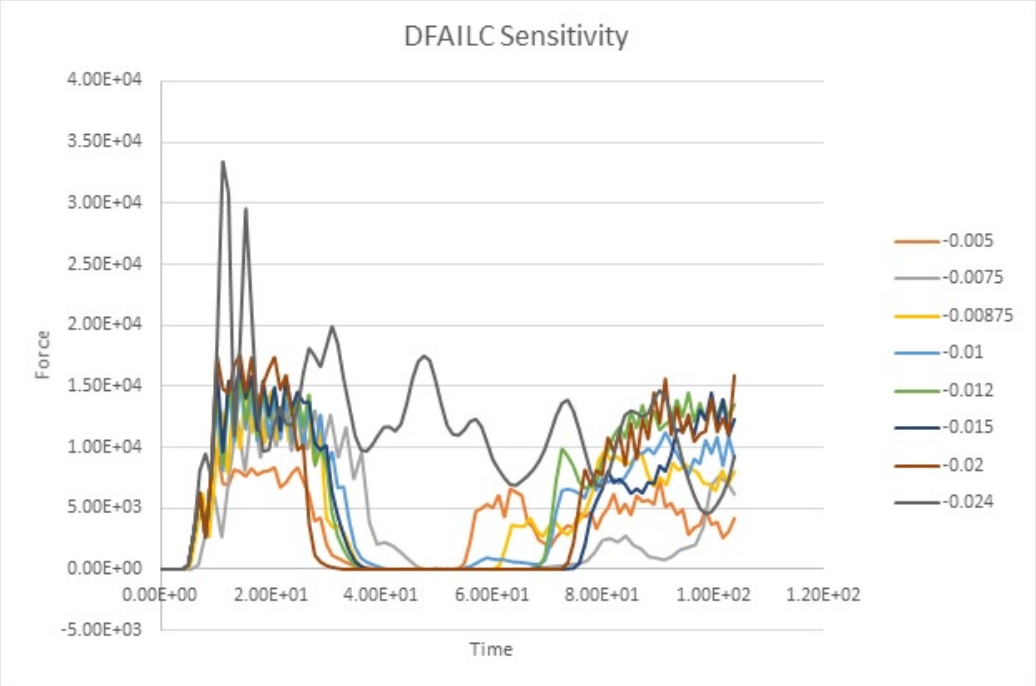

Fig. 4.12. Sensitivity Analysis of varying DFAILC

dramatically. The effect on structure is negligible. As MAT 54 involves Chang-Chang failure criterion, the stresses are the focus of failure. By increasing the strains, the stress limits are varied which increases the force requirements for element failure. From various trials the DFAILC selected was -0.01207.

Effect of varying DFAILM

The strain in transverse direction is dependent on both fibers and matrix. The effects of DFAILM are of great interest in unidirectional fibers as the transverse direction failure is governed by matrix failure and hence DFAILM is crucial. However, in fabric the DFAILM does not contribute as the primary failure mode in lateral direction. As shown in Figure 4.13, the effects of DFAILM has no effects and hence is not considered for further variations to correlate.

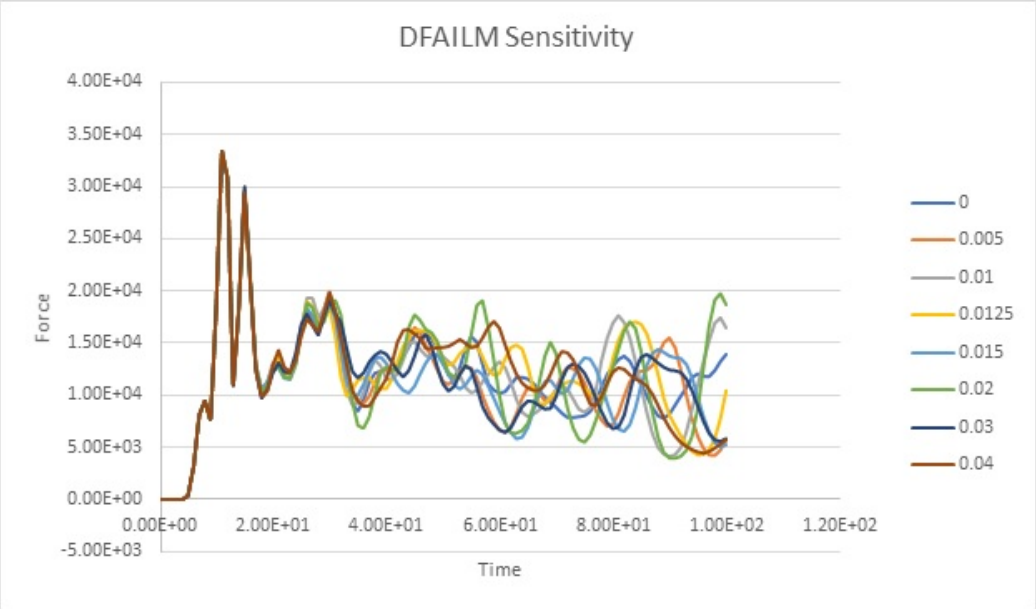

Fig. 4.13. Sensitivity Analysis of varying DFAILM

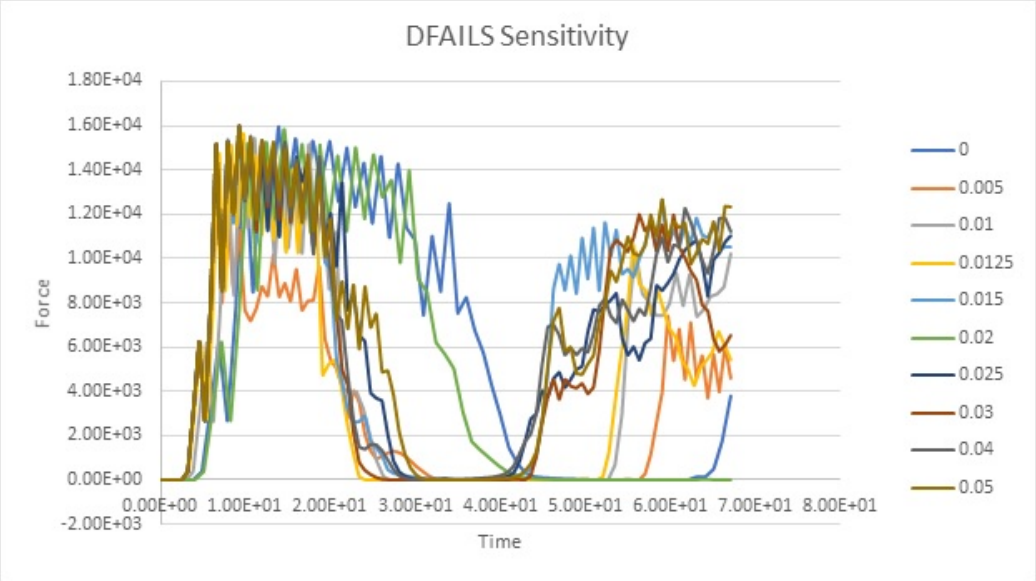

Fig. 4.14. Sensitivity Analysis of varying DFAILS

Effect of varying DFAILS

If the primary failure criterion is shear strength, then the effects of shear strain is of great interest. Figure 4.14 shows the effects of varying strain. In general, the effects of strain have little variations on the force.

Effect of varying EFS

EFS strain is utilized to generalize the strain values for the material model. However, if the strain values are mentioned in DFAILT, DFAILC OR DFAILM are defined then it is not completely utilized. The effects of EFS are shown in Figure 4.15. For large increments in EFS there is no significant improvement and hence is not the major factor for consideration.

By analyzing the effects of strain variations on force-displacement curves, we can conclude that the compressive strain plays the most important role and is the crucial factor in composite failure. The compressive strain and strength determine the failure effects in compression tests as is expected. However, the effects of tension and shear

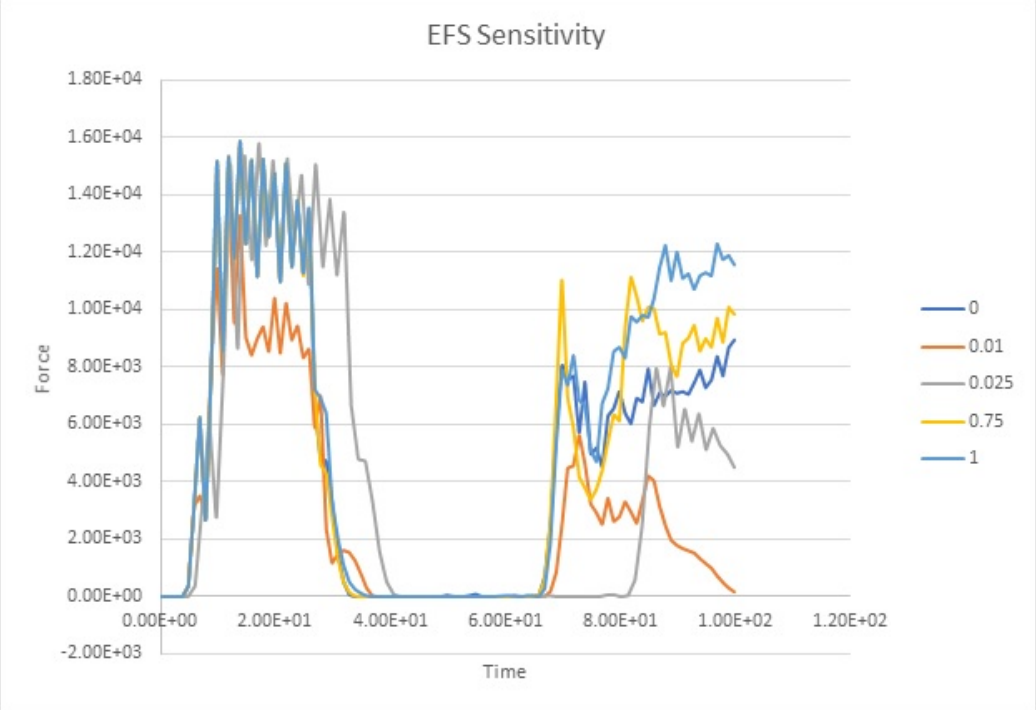

Fig. 4.15. Sensitivity Analysis of varying EFS

have very low significance. In order to correctly correlate the experimental tests, other parameters need to be considered and varied to achieve suitable results. Parameters that control the compressive nature of material will have the most effects and hence have to be calibrated correctly and accurately.

4.1.3 Sensitivity Analysis of model specific parameters

Effect of varying ALPHA and BETA

Alpha parameter determines the shear behavior in the large deformation space. It modifies the shear behavior by adding a third order non-linear term in the basic shear formulation. However, the effects of varying alpha have little positive effects on the load curve. This can be attributed to the little significance of shear parameter on failure of composite specimen. As can be seen in Figure 4.16, large variations have little effects hence a value of 1 is chosen. BETA is also a parameter which affects the shear formulation characteristics and hence shouldnt affect the simulation in any major way. The effect of BETA=0 signifies Maximum Stress criterion for fiber tensile failure and BETA = 1 signifies Hashims failure criterion. As these parameters have small effects, the failure mechanism is not governed by these failure criterions. These results are in agreement with previous results which suggest tension and shear failure as not being the primary failure mechanism.

Effect of varying TFAIL

TFAIL is time-step for element deletion after failure. As the value of TFAIL varies there is no significant impact on force curve. However, if TFAIL is larger than time-step, then the elements are deleted before complete loading which lead to unstable crushing and failure. The effects of varying TFAIL is indicated in Figure 4.17.

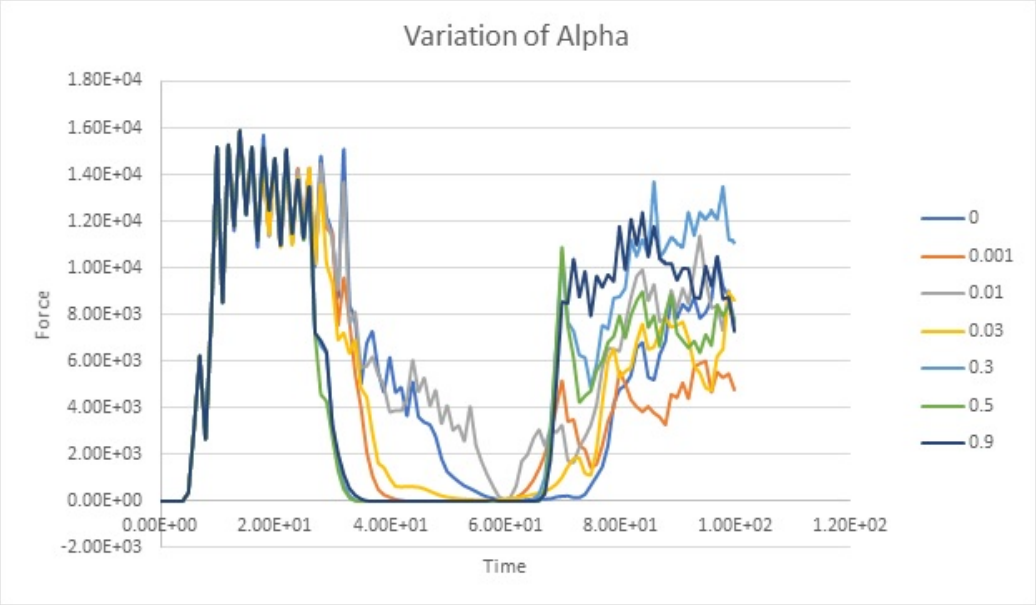

Fig. 4.16. Sensitivity Analysis of varying parameter Alpha

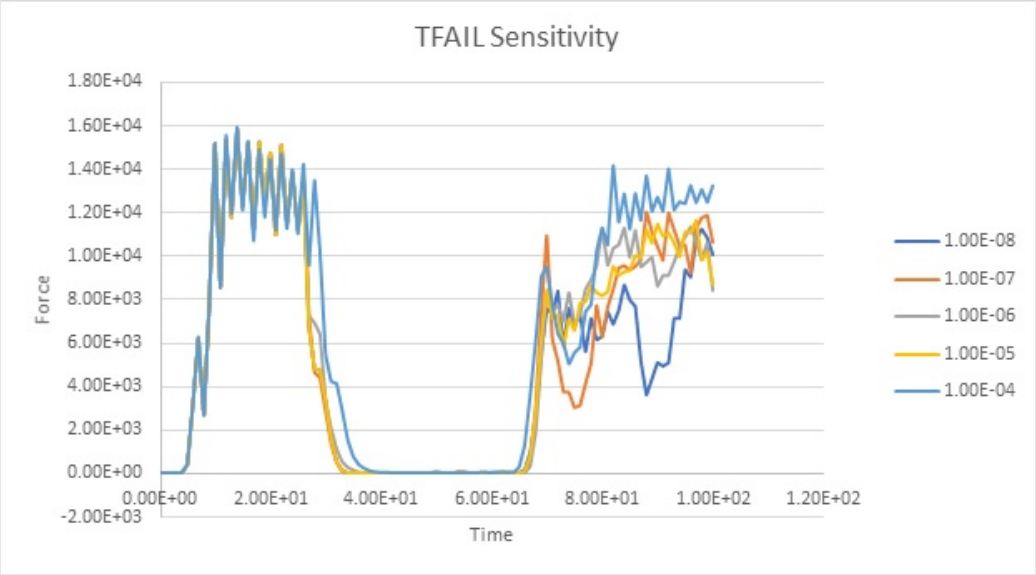

Fig. 4.17. Sensitivity Analysis of varying parameter TFAIL

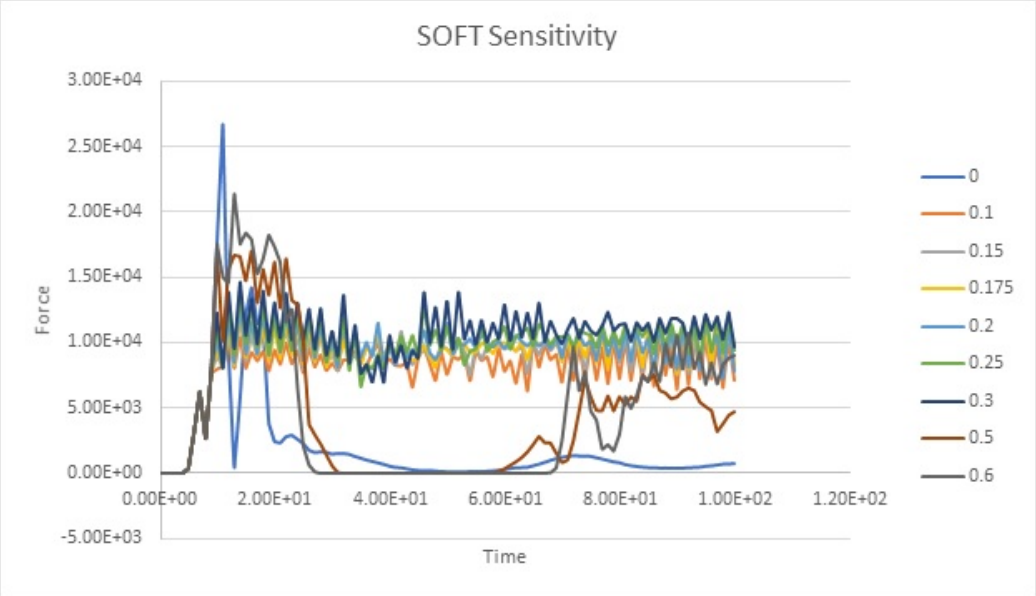

Fig. 4.18. Sensitivity Analysis of varying parameter Soft

Effect of varying Soft

The most important and influential criterion for determining a good correlation is the parameter SOFT. As the value of SOFT increases there is progressive crushing. This is due to reduction in strength in row of elements immediately after the crush front. As the value of SOFT increases from the strength in elements increases which may lead to significant load transfer and global buckling. In Figure 4.18, at SOFT=0 the strength in the elements is reduced to 0 which leads to drastic failure. By increasing the SOFT to 0.1 the force curve stabilizes to around 8500 N. Further increments increase the average crush load. This increment is observed till SOFT=0.3. Further increase leads to global buckling and drastic failures. From the data we can fixate the value of SOFT to 0.15 as it provides values close to that achieved in experiments.

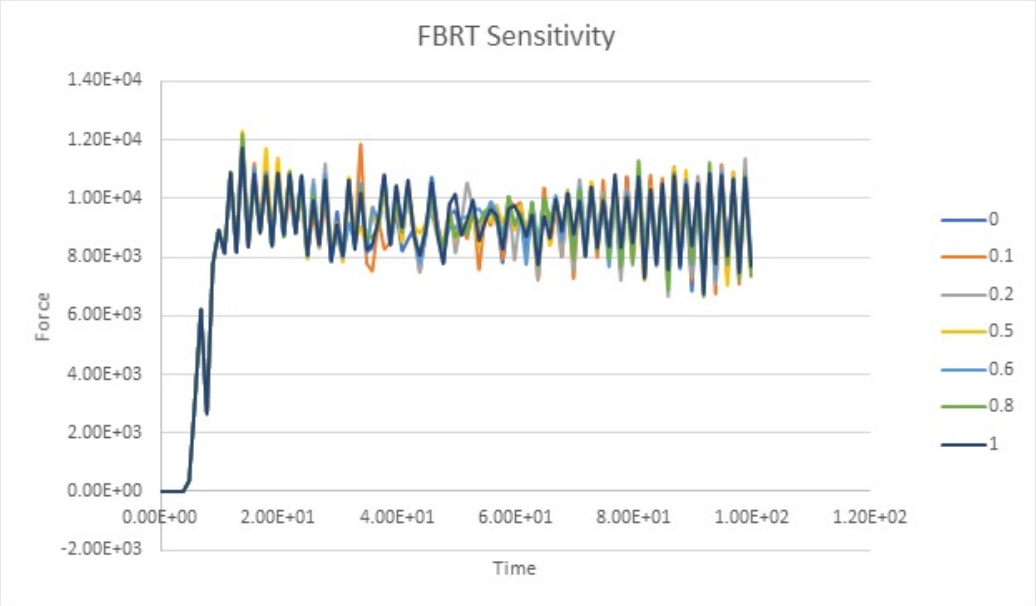

Fig. 4.19. Sensitivity Analysis of varying FBRT

Effect of varying FBRT

FBRT is the softening factor or reduction factor for fiber strength in tension after the element is subjected to a force and there is a deletion of a particular integration point or deletion of a particular ply. As the simulation reliance on the tension failure is not significant, the effects of FBRT are not significant. This can be seen in Figure 4.19 wherein the factor ranges from 0 to 1 with little to no effect on force curve.

Effect of varying YCFAC

The other factor which degrades the fiber strength in the same element is YCFAC. It is attributed to strength reduction factor for the compressive strength after a ply has been damaged or failed. As can be expected, the effects of YCFAC are significant on the force curve. From the Figure 4.20, it can be observed as the value of YCFAC increases, the reduction in strength increases. This further increases the force requirements as the progressive damage is enhanced. The force required to fail the rest

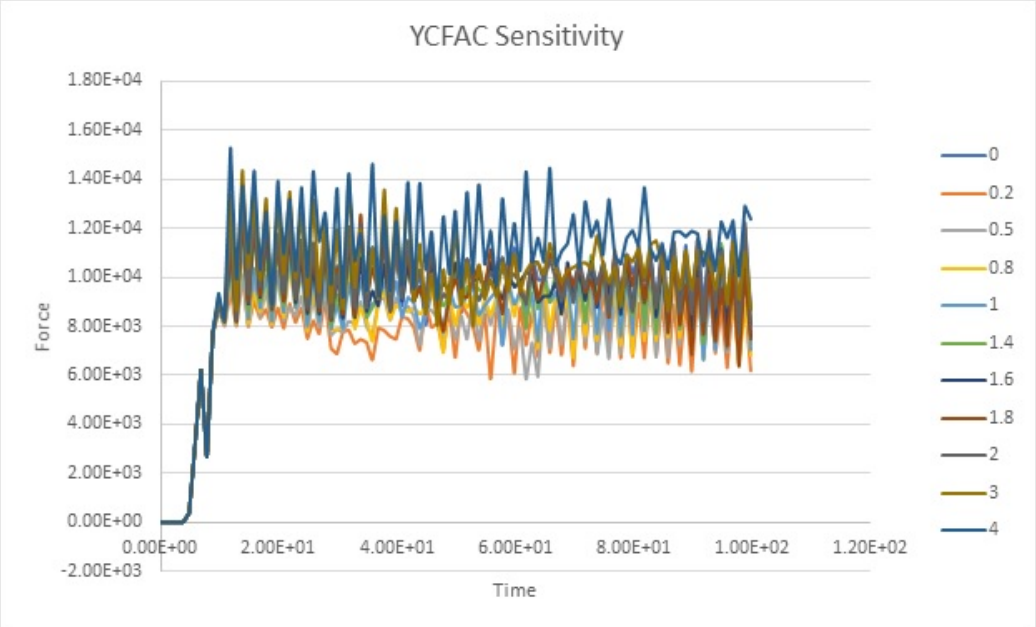

Fig. 4.20. Sensitivity Analysis of varying YCFAC

of plies in an element reduces, this along with SOFT parameter enable the elements to interact in similar way as observed in experiments. The effects of delamination and fronds are simulated by utilizing these parameters. From the sensitivity analysis conducted the value of YCFAC is finalized to 3.

Effect of varying Contact Load Curve

The contact curve has a large effect on the stability and failure of structure. There is however no research conducted on the derivation of the load curve. The four curves presented in this research are obtained by trial and error and they are specific for this particular geometry and material. However, these curves will provide a good baseline for more complex structures and hence help better estimate the stacking sequence for a structure. Furthermore, complex composite crash structures often include large factor of safety to incorporate for such variations in simulations. As can be seen in Figure 4.21, there are four curves each of different exponential stiffnesses. As the

Fig. 4.21. Four loading curves for contact definition

penetration of rigid body into the element increases the forces exerted on the nodes of elements are determined by the loading curve. As can be observed in Figure 4.22, the stiffer the loading curve lesser is the average crushing force. This is due to element deletion and failure due to the sudden increase in force being applied at the nodes. In the case of soft curve, the load applied is less gradual leading to more gradual force transfer which allows all the elements to evenly distribute the load before there is a failure of row of elements. Thus, a stiffer curve will have lesser average crushing force. However, in this case, the stiffer curve (Stiff 2) predicts the experimental results more accurately and was hence selected.

Effect of varying Trigger Thickness

The trigger geometry and thickness directly affect the stability and peak load exerted on the specimen. A correct representation of trigger is necessary to initiate stable and progressive crushing. In the experiments conducted the trigger geometry

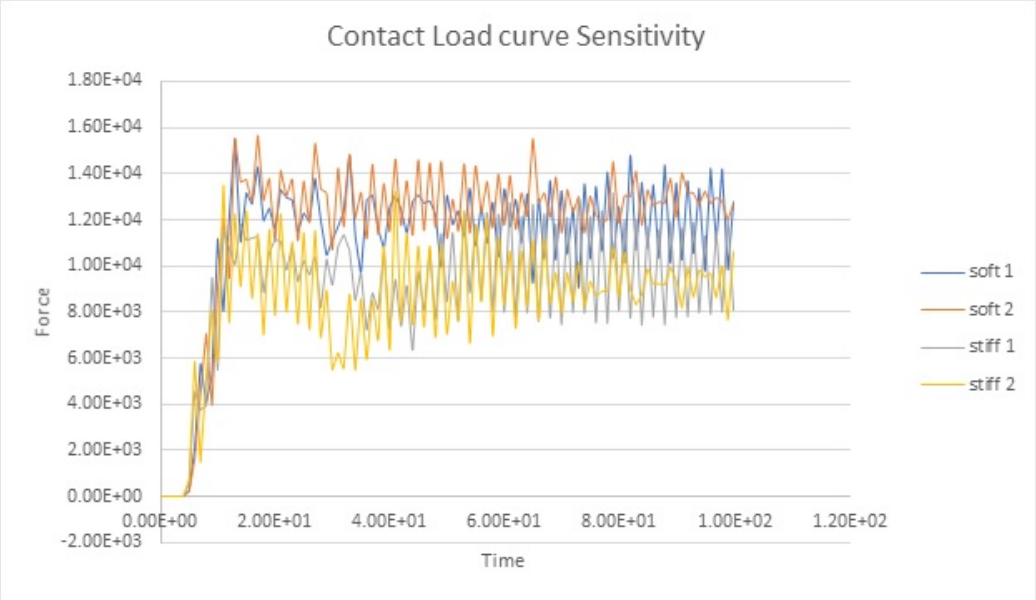

Fig. 4.22. Effect of contact loading curve on force curves

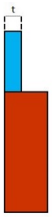

Fig. 4.23. Trigger thickness in simulation

is a 45 chamfer. It is not ideal for creating a solid geometry with the chamfer just to correctly replicate the experimental geometry. In simulations, the geometry of a trigger is often chosen as shown in Figure 4.23. With the help of varying ply thickness, the behavior of trigger can be replicated in composite structures. The thickness values chosen varied between 0.05 mm to 0.4 mm. As the thickness of the cured laminate in experiments equaled to 1 mm the thickness of trigger simulated varied from 5% to 40%. As can be seen in Figure 4.24, the increase in trigger thickness from 5% to 18% increased the peak force applied on the structure drastically. Any further increments in the thicknesses resulted in failure of a particular element followed by deletion of entire row of elements. This resulted in a constant progressive failure for 0.3 mm trigger thickness. However, on further increase in thickness, the strength in some elements was reduced due to large sudden force transfer. Thus, the structure experienced global buckling and failed drastically. From all the data available, the trigger step with 0.2 mm thickness best suited the simulation resulting in stable, progressive crushing.

Effect of varying Trigger Layup

As mentioned earlier, the trigger stacking sequence or ply sequence is varied in order to replicate or simulate the workings of trigger as observed in experiments. By utilizing the property of asymmetric ply sequence, the lamina bending of trigger can be varied thus simulating a 45 chamfer. Although the effects of such variations would

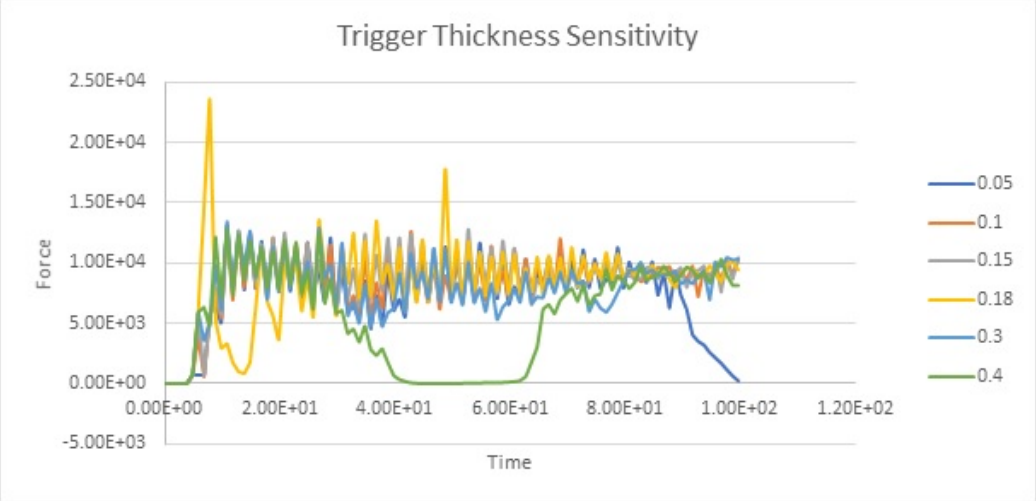

Fig. 4.24. Trigger thickness variation in LS-DYNA simulations

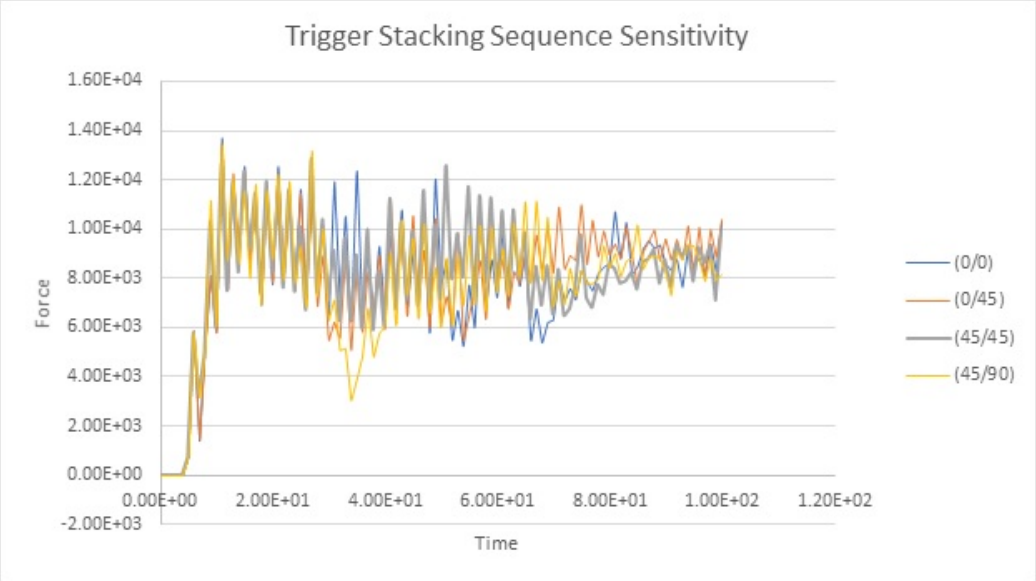

Fig. 4.25. Sensitivity Analysis of Trigger stacking sequence

be negligible due to only two plies, a stable and progressive crushing was observed in (0,45). The effects of ply variation are shown in Figure 4.25. As can be observed, the trigger stacking sequence plays an important role in stability and progression of crushing. By considering the experimental force curve, the stacking sequences (0/0), (45/90), and (45/45) were not chosen.

Table 4.4.: Finalized MAT 54 Material model values

Parameter	Value	Unit
MAT 54: XT	794	MPa
MAT 54: XC	796	MPa
MAT 54: YC	775	MPa
MAT 54: YT	766	MPa
MAT 54: SC	78	MPa
DFAILT	0.01203	-
DFAILC	-0.01207	-

continued on next page

Table 4.4.: *continued*

Parameter	Value	Unit
DFAILM	0.011785	-
DFAILS	0.01852	-
EFS	0	-
ALPHA	1	-
BETA	0.5	-
TFAIL	1E-9	-
SOFT	0.15	-
FBRT	1	-
YCFAC	3	-
CONTACT LOAD-CURVE	STIFF 2	-
TRIGGER THICKNESS	0.2	mm
TRIGGER LAYUP	(0,45)	-

5. FINAL GEOMETRY ANALYSIS

From the coupon tests conducted earlier, we can now analyze and simulate the failure mechanism in more complex geometries. The purpose of earlier design modelling was to finalize all parameters necessary to accurately model and simulate the large deformations occurring in the structures. The structure to be assessed is a Formula 3 nosecone. It would have to meet the requirements set by FIA to ensure the safety of driver in a racing car. The geometry is shown in Figure 5.1.

5.1 Objective

According to the rules of FIA Formula 3, the frontal impact test needs to be carried out at a speed of 14 m/sec with a test sled weighing 600kgs. The rules specify

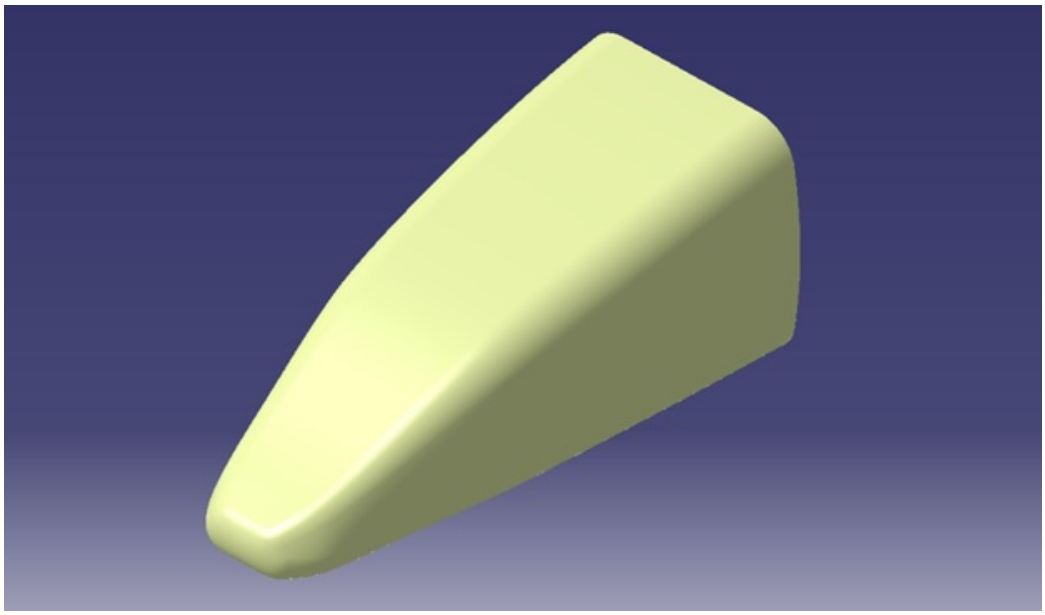

Fig. 5.1. CAD geometry of Formula 3 nosecone

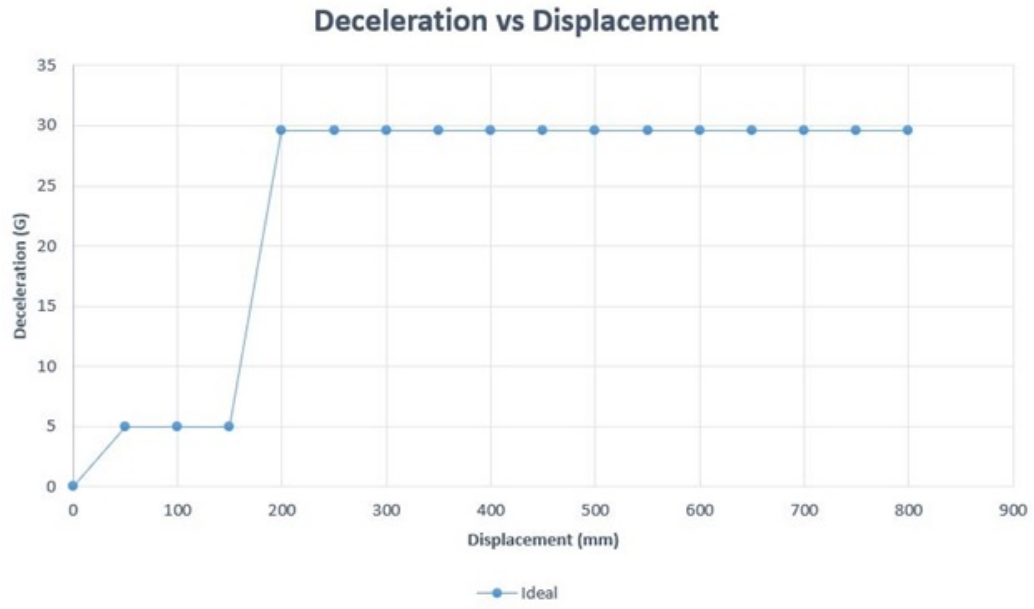

Fig. 5.2. Deceleration limits set by FIA for Formula 3 nosecone

the deformable part to decelerate at a maximum of 5gs for the first 150mm and an overall average g-force to be lower than 25g including the first 5g limit, Figure 5.2. Furthermore, the entire velocity of the vehicle needs to be dissipated without the failure of any other component of the survival cell. Also, a nose push-off test is carried out to regulate the failure of nosecone for an angle impact. This test is out of scope for this research, as it more aligns with static analysis of component.

5.2 Sections

The geometry of nosecone is divided into two parts- the cover and the cone. The cover is not included in the simulations as this part would be manufactured bonded separately with the crash structure. Also, since this part will not be cured with the rest of the structure it lacks the structural integrity and consistent manufacturing process to evaluate the effects on deceleration. As can be seen in Figure 5.3, the part does not include the cover. Furthermore, the remaining geometry is divided into 21 sections each averaging around 30 mm in width. The number of sections

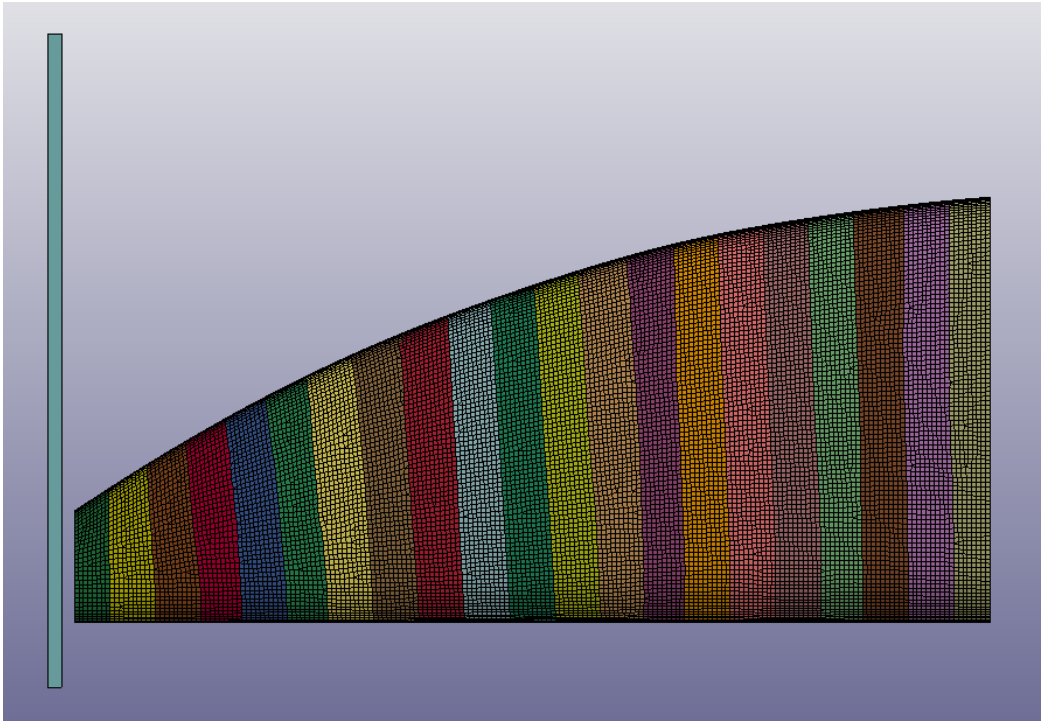

Fig. 5.3. Sections created for the Formula 3 nosecone

were considered based on manufacturing processes. Furthermore, the sections were divided only longitudinally as the research focuses on a 0 angle of impact. Each section is individually defined to have a particular layup sequence, ply thickness and ply orientation. The design is completed with each section acting as a trigger for the proceeding section, thus leading to stable and controlled crushing as well as controlling the deceleration peaks. This methodology is intended for a dual application of reducing the value of the force peak and initializing structure collapse in a stable regime.

5.3 Stacking Sequence

From the experimental tests conducted, the average SEA value was found out to vary around 35 J/gm, Figure 3.6. By utilizing the particular SEA value, and by considering the variations in SEA as a function of percentage cross-sectional curvature

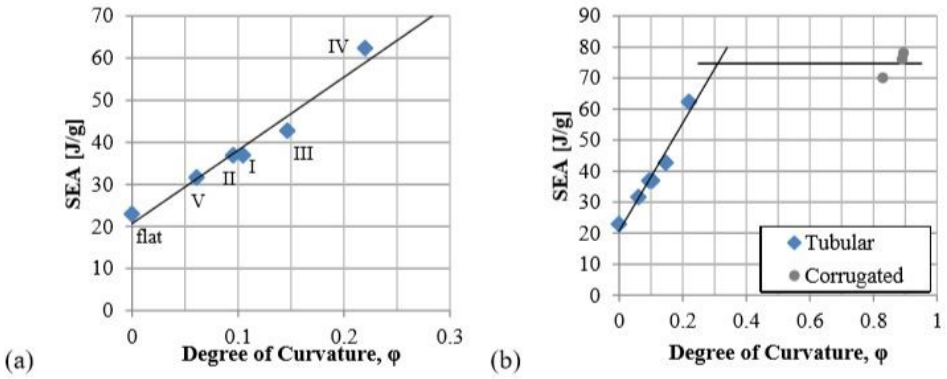

Fig. 5.4. SEA vs ϕ variation mentioned by Wade [21]

[21], we can conclude the variations in SEA of SC110 (T2) 2 X 2 twill Carbon Fiber to vary as shown in Figure 5.4. The energy absorption requirements can be obtained from the ideal deceleration curve which would ensure the limits set in Figure 5.2 are not violated. By calculating the average curvature percentage in each section, we can calculate the maximum SEA by following the curves in Figure 5.4. We can thus find the number of layers by calculating the mass requirements in each section by utilizing density, surface area and SEA.

The natural geometry of the structure enables an increase in deceleration as the structure collapses. This is due to an increase in total material available to collapse. However, the increase in cross-sectional area does not meet the energy absorption requirements set by FIA and hence the structure requires varying number of layers and an increase in number of layers as the deformation within the structure increases. The sectional stacking sequence is presented in Table 5.1. There is an error in calculated and resultant stacking sequence, this is further explained in next section.

Table 5.1.: Stacking sequence in Formula 3 nosecone sections

Section ID	Initial Layup	Final Layup
1	2*(0/90)	3*(0/90)
2	3*(0/90)	5*(0/90)
3	5*(0/90)	8*(0/90)
4	5*(0/90)	8*(0/90)
5	6*(0/90)	8*(0/90)
6	7*(0/90)	9*(0/90)
7	8*(0/90)	10*(0/90)
8	9*(0/90)	11*(0/90)
9	11*(0/90)	12*(0/90)
10	12*(0/90)	13*(0/90)
11	13*(0/90)	14*(0/90)
12	14*(0/90)	15*(0/90)
13	15*(0/90)	16*(0/90)
14	16*(0/90)	17*(0/90)
15	17*(0/90)	18*(0/90)
16	18*(0/90)	19*(0/90)
17	19*(0/90)	20*(0/90)
18	20*(0/90)	21*(0/90)
19	22*(0/90)	22*(0/90)
20	22*(0/90)	22*(0/90)
21	24*(0/90)	24*(0/90)

5.4 Errors

While the SEA calculations lead to a particular stacking sequence, the previous research failed to consider the angle of attack β and its impact on energy absorption capacity. As the geometry considered had an extreme angle of attack, the calculations failed to accurately represent the correct SEA. This is due to the dominance of lamina bending due to its natural angle of attack in one of the sides of the truncated pyramidal cone. However, the sections with negligible β had better estimations of SEA and could approximately predict the right ply sequence. Furthermore, as the angle of attack increased the error in ply sequence estimation increased hence indicating a direct relation between SEA and angle of attack.

Table 5.2.: Layup Error variations with Angle of attack

Section ID	Initial Layup	Final Layup
1	1	32.5
2	2	30.5
3	3	28.3
4	3	25.8
5	2	23.3
6	2	21.2
7	2	19
8	2	17
9	1	14
10	1	12.8
11	1	11.6
12	1	10.5
13	1	9.6
14	1	8.9

continued on next page

Table 5.2.: *continued*

Section ID	Initial Layup	Final Layup
15	1	8.3
16	1	7.9
17	1	7.2
18	1	6.8
19	0	6.3
20	0	5.7
21	0	5.5

5.5 Deceleration Curve

The resultant deceleration vs displacement curve, Figure 5.5, shows that in the first 150 mm of crushing, the deceleration was stabilized to 0.04 mm/ms^2 or 4g. An average deceleration of 12.45g was observed, which is within the 25g limit imposed by the rules. As there are no sudden dips or increases in the forces exerted on the structure, it can be concluded that the deformable structure collapses continuously. It was observed that an initial kinetic energy of 58.8kJ was completed dissipated into splaying/fragmentation of fibers and into heat energy generated due to friction between the surfaces. The methodology of varying the number of plies with displacement, resulted in an optimized crash structure which met the rules and regulations imposed by FIA.

5.6 Honeycomb Structures

Although the use of above monolithic structure is suitable for crashworthiness, the number of layers and complexity of layup increases the manufacturing time and costs. Furthermore, the use of honeycomb structures increases the bending resistance

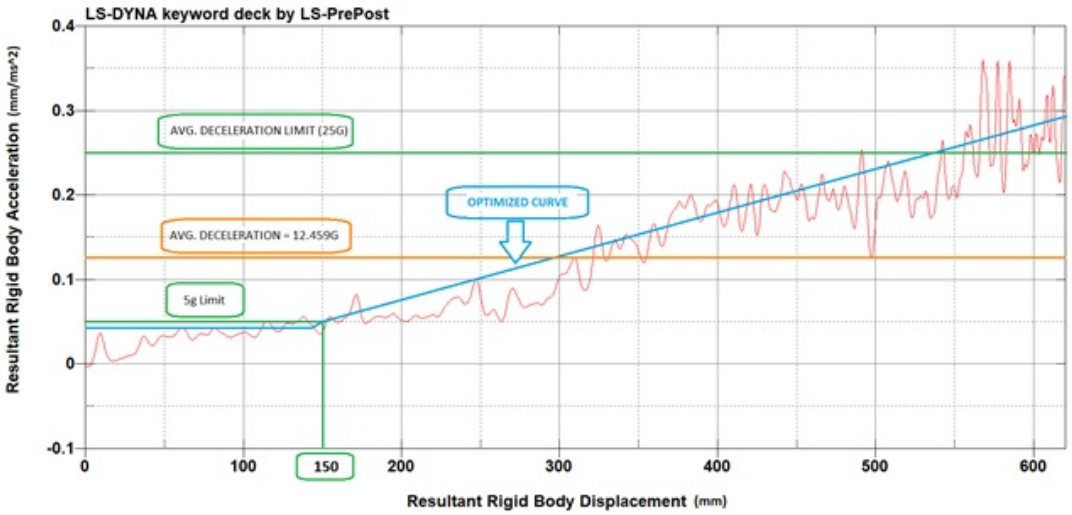

Fig. 5.5. Resultant deceleration curve for Monolithic Formula 3 nosecone

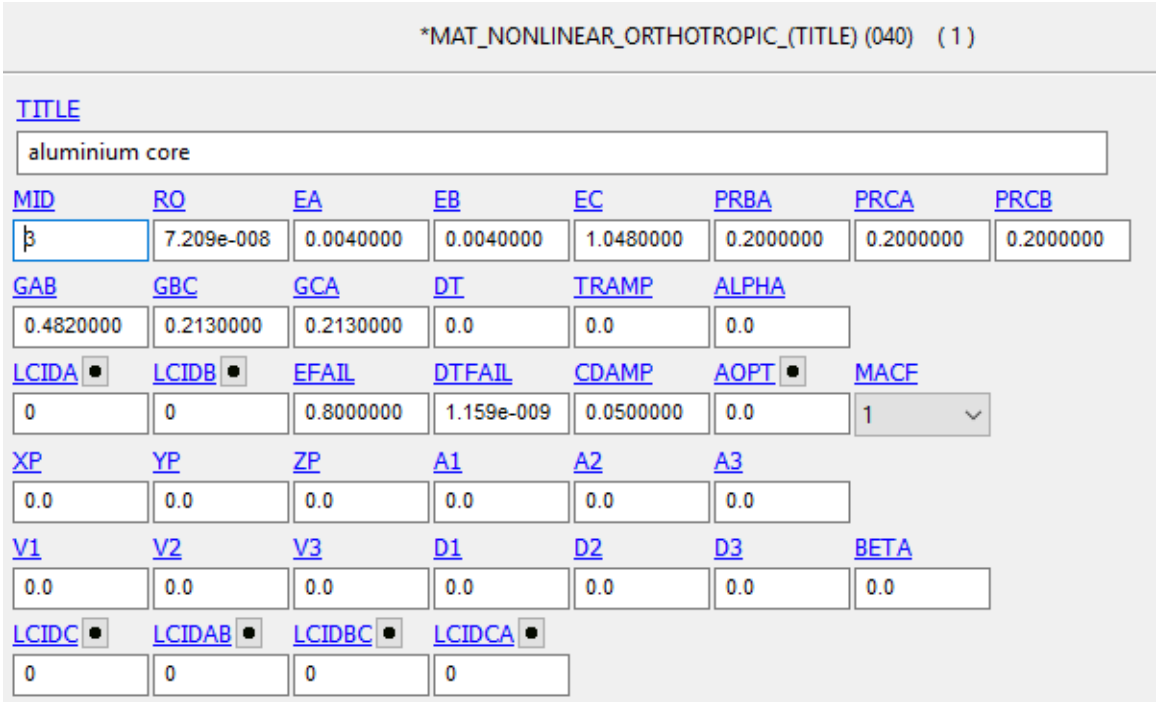

Fig. 5.6. Material model Datasheet for Aluminium Honeycomb

which is a major drawback in nosecone structures. The use of honeycomb structure subjects the individual laminas to higher strains and stresses as the plies are more separated from the mid-plane. The following Table 6 shows the stacking sequence utilized. There are two ways of incorporating a honeycomb structure. One would be the use of machined honeycomb structure and the other is the utilization of standard honeycomb thickness. The material model utilized for honeycomb structure is MAT 40 Nonlinear Orthotropic. The material model data sheet is shown in Figure 5.6.

Table 5.3.: Stacking sequence for composite nosecone with variable core

Section ID	Outer Skin	HC (mm)	Inner Skin
1	2*(0/90)	-	2*(0/90)

continued on next page

Table 5.3.: *continued*

Section ID	Outer Skin	HC (mm)	Inner Skin
2	3*(0/90)	-	3*(0/90)
3	4*(0/90)	-	4*(0/90)
4	4*(0/90)	-	4*(0/90)
5	4*(0/90)	-	4*(0/90)
6	4*(0/90)	1	4*(0/90)
7	4*(0/90)	3	4*(0/90)
8	4*(0/90)	5	4*(0/90)
9	4*(0/90)	7	4*(0/90)
10	4*(0/90)	9	4*(0/90)
11	4*(0/90)	10	4*(0/90)
12	4*(0/90)	10	4*(0/90)
13	4*(0/90)	10	4*(0/90)
14	4*(0/90)	10	4*(0/90)
15	4*(0/90)	10	4*(0/90)
16	4*(0/90)	10	4*(0/90)
17	4*(0/90)	10	4*(0/90)
18	4*(0/90)	10	4*(0/90)
19	4*(0/90)	10	4*(0/90)
20	4*(0/90)	10	4*(0/90)
21	4*(0/90)	10	4*(0/90)

Table 5.4.: Stacking sequence for composite nosecone with constant core

Section ID	Outer Skin	HC (mm)	Inner Skin
1	2*(0/90)	-	2*(0/90)
2	3*(0/90)	-	3*(0/90)
3	4*(0/90)	-	4*(0/90)
4	4*(0/90)	-	4*(0/90)
5	4*(0/90)	-	4*(0/90)
6	4*(0/90)	10	4*(0/90)
7	4*(0/90)	10	4*(0/90)
8	4*(0/90)	10	4*(0/90)
9	4*(0/90)	10	4*(0/90)
10	4*(0/90)	10	4*(0/90)
11	4*(0/90)	10	4*(0/90)
12	4*(0/90)	10	4*(0/90)
13	4*(0/90)	10	4*(0/90)
14	4*(0/90)	10	4*(0/90)
15	4*(0/90)	10	4*(0/90)
16	4*(0/90)	10	4*(0/90)
17	4*(0/90)	10	4*(0/90)
18	4*(0/90)	10	4*(0/90)
19	4*(0/90)	10	4*(0/90)
20	4*(0/90)	10	4*(0/90)
21	4*(0/90)	10	4*(0/90)

As can be observed in Figures 5.7 and 5.8, the use of honeycomb increases the deceleration curve significantly. As the compressive strength of honeycomb is negligible, the deceleration is achieved in lesser amount of carbon fiber material. This is

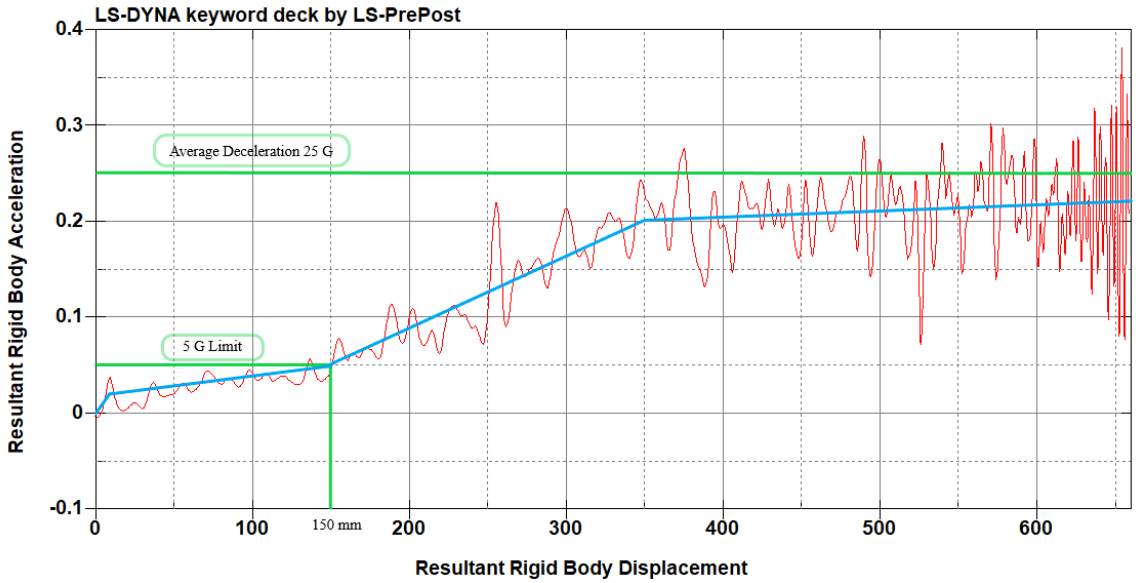

Fig. 5.7. Deceleration curve for variable honeycomb core thickness in Formula 3 nosecone

due to reduction in fiber splaying/bending and increase in fragmentation. Furthermore, a controlled sudden increase in deceleration results in lesser peak deceleration. Although the average deceleration increases as compared to monolithic structures, it is well within the limits of FIA regulations and hence acceptable.

Figure 5.7 shows the simulated deceleration curves for a variable core thickness. Although the core thickness increase is achieved in 5 steps rather than a gradual chamfer, the effect on deceleration curve is gradual. An average of 4 g is observed in the first 150 mm which is almost consistent with all the models. The rate of increase henceforth is more than that observed in monolithic structure. The deceleration stabilizes to 21 g after around 55% collapse which is still within the safety limits. Furthermore, the collapse of structure is uniform and stable hence indicating progressive and constant composite collapse without the issues of global buckling.

Figure 5.8 shows the simulated deceleration curves for a constant core thickness. The simulation neglects the effects of any epoxy pockets or voids within the structure

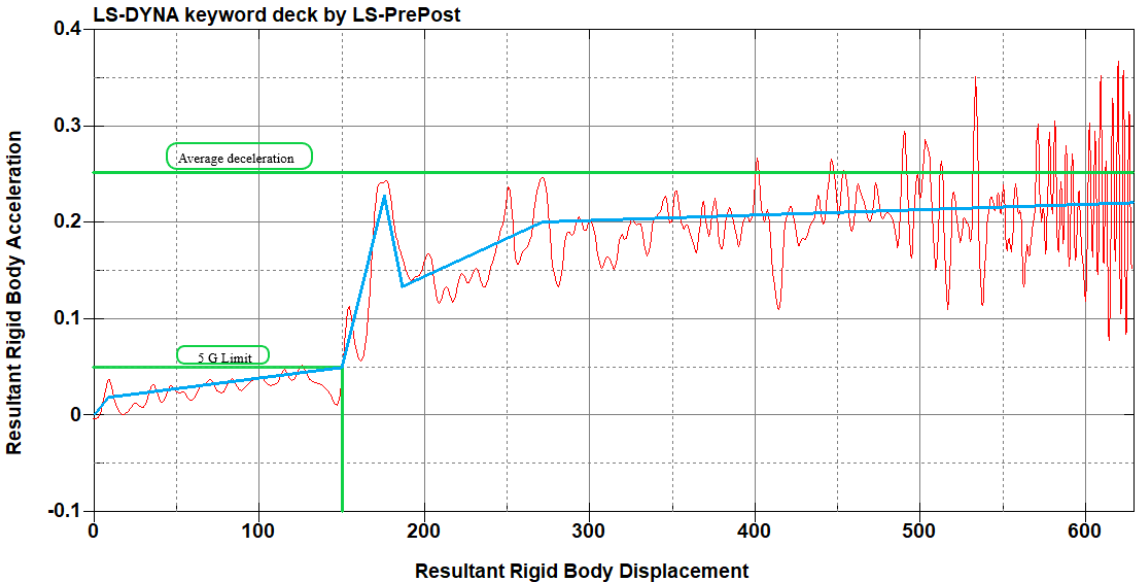

Fig. 5.8. Deceleration curve for constant honeycomb core thickness in Formula 3 nosecone

due to such sudden separation between the plies. As is evident in the deceleration curve, the impact of section with honeycomb increases the deceleration from 5g to 24g within the collapse of next section. This is a common observation within structures having very high stiffness or very high increase in stiffness in optimized structures. After the first initial impact the rows of elements adjacent to crush front are often deleted due to failure of certain element. Thus, there is a dip in deceleration, which later stabilizes to a constant value of around 21 g.

From the deceleration curves simulated in Figures 5.5, 5.7 and 5.8 we can conclude that the failure of composite structure results in safe and predictable collapse which are within the limits imposed by FIA and hence can successfully utilized as per the design and manufacturing requirements of the vehicle.

6. CONCLUSION

From the experimental research conducted on material, SC 110 (T2) 2 X 2 twill Carbon Fiber, it can be concluded that the quasi-static compression tests on square tubes can accurately predict the Specific Energy of Absorption for a particular geometry. The experiments showed good correlation with previous experimental results conducted on similar structures. The experiments also showcased the importance of a good trigger mechanism which is essential for achieving progressive crushing. The use of chamfered edge initiated the failure and suppressed other failure mechanisms like delamination and global buckling. The understanding of trigger mechanism played an important in determining the ply stacking sequence in various sections of monolithic structures, as each section acts as a virtual trigger for the adjacent section.

The simulation of compression tests in LS-DYNA MAT 54 also indicated the strong reliance of experimental parameters like SOFT, YCFAC, Contact Load Curve, XC and trigger thickness on the overall results. Without the right calibration of these parameters, the failure of structure greatly varies from the experiments and hence leads to wrong design considerations. An extensive sensitivity analysis in MAT 54 revealed the strong reliance of simulation model on compression parameters only. The effects of all other parameters where negligible.

The simulation of complex structures was conducted once the particular simulation model was verified with the experimental results. The model was divided into longitudinal sections each with independent stacking sequence. The simulation results suggested an error in the SEA calculations which only considered the effects of cross-sectional curvature percentage. The error in SEA was observed to be directly dependent on the angle of attack of the section. Hence by reconsidering the stacking sequence, a controlled collapse of nosecone structure was achieved, with a significant margin of safety to the limits mentioned by FIA. Furthermore, by analyzing various

design concepts like constant core thickness and variable core thickness, it can be concluded that the monolithic model provided the best results considering the lowest weight of all cases. However, due to the time and cost constraints involved during manufacturing, the variable core thickness model provided the best cost-effective results.

REFERENCES

REFERENCES

[1] C. Nailadi, "A summary of the acc tube testing program," in *Proceedings of the 49th MIL-HDBK-17 Coordination Meeting-Crashworthiness Working Group, Santa Monica, CA*, 2005.

[2] A. Browne, N. Johnson, and M. Botkin, "Dynamic crush response of composite crash boxes: effects of impact angle and bumper attachment," in *Proceedings of the ASC 27th Technical Conference*, 2010.

[3] C. Bisagni, "Experimental investigation of the collapse modes and energy absorption characteristics of composite tubes," *International journal of crashworthiness*, vol. 14, no. 4, pp. 365–378, 2009.

[4] R. Jeryan, "Energy management working group activities," in *Proceedings of the 48th MIL-HDBK-17 Coordination Meeting - Crashworthiness Working Group, Charlotte, NC*, Mar. 2005.

[5] D. Hull, "A unified approach to progressive crushing of fibre-reinforced composite tubes," *Composites science and technology*, vol. 40, no. 4, pp. 377–421, 1991.

[6] A. K. Pickett, T. Pyttel, F. Payen, F. Lauro, N. Petrinic, H. Werner, and J. Christlein, "Failure prediction for advanced crashworthiness of transportation vehicles," *International Journal of Impact Engineering*, vol. 30, no. 7, pp. 853–872, 2004.

[7] P. D. Bois, "Crashworthiness engineering with ls-dyna," in *FEA Information International News for the World-Wide Engineering Community*, December 2001.

[8] G. L. Farley, "Energy-absorption capability of composite tubes and beams," Ph.D. dissertation, Virginia Polytechnic Institute and State University, 1989.

[9] G. L. Farley and R. M. Jones, "Crushing characteristics of continuous fiber-reinforced composite tubes," *Journal of composite Materials*, vol. 26, no. 1, pp. 37–50, 1992.

[10] J. J. Carruthers, A. Kettle, and A. Robinson, "Energy absorption capability and crashworthiness of composite material structures: a review," *Applied Mechanics Reviews*, vol. 51, no. 10, pp. 635–649, 1998.

[11] H. Hamada, J. Coppola, D. Hull, Z. Maekawa, and H. Sato, "Comparison of energy absorption of carbon/epoxy and carbon/peek composite tubes," *Composites*, vol. 23, no. 4, pp. 245–252, 1992.

[12] (CMH-17), *Composite Materials Handbook*, rev. g., vol. 3, chapter 16 ed., 2012.

[13] E. L. Fasanella, K. E. Jackson, and K. H. Lyle, "Finite element simulation of a full-scale crash test of a composite helicopter," *Journal of the American Helicopter Society*, vol. 47, no. 3, pp. 156–168, 2002.

[14] E. L. Fasanella and K. E. Jackson, "Best practices for crash modeling and simulation," National Aeronautics and Space Administration and Langley Research Center (U.S.), Hampton, VA, Tech. Rep., October 2002.

[15] A. F. Johnson, A. K. Pickett, and P. Rozycki, "Computational methods for predicting impact damage in composite structures," *Composites Science and Technology*, vol. 61, no. 15, pp. 2183–2192, 2001.

[16] L. G. Maia and P. H. I. A. De Oliveira, "A review of finite element simulation of aircraft crashworthiness," SAE Technical Paper, Tech. Rep., 2005.

[17] K. E. Jackson and E. L. Fasanella, "Development of an ls-dyna model of an atr42-300 aircraft for crash simulation," in *Proceedings of the 8th International LS-DYNA User's Conference, Detroit, MI*, May 2004.

[18] A. Byar, "A crashworthiness study of a boeing 737 fuselage section," Ph.D. dissertation, Drexel University, 2004.

[19] S. Heimbs, M. Hoffmann, M. Waimer, S. Schmeer, and J. Blaurock, "Dynamic testing and modelling of composite fuselage frames and fasteners for aircraft crash simulations," *International Journal of Crashworthiness*, vol. 18, no. 4, pp. 406–422, 2013.

[20] P. Feraboli, "Development of a corrugated test specimen for composite materials energy absorption," *Journal of Composite Materials*, vol. 42, no. 3, pp. 229–256, 2008.

[21] B. Wade, "Capturing the energy absorbing mechanisms of composite structures under crash loading," Ph.D. dissertation, 2014.

[22] LSTC, *LS-DYNA Keyword User's Manual Version 971*, May 2007.

[23] M. Paz, "Structural dynamics theory and computation," in *New York: Van Nostrand Reinhold*, 1991.